MATHEMATICAL MODELING AND SIMULATION OF A MULTISCALE TUMOR INDUCED ANGIOGENESIS MODEL

---

by

Richard C Ewool

A Dissertation

Presented to the Faculty of the Department of Computational Sciences

Middle Tennessee State University

August 2016

In Partial Fulfillment

of the Requirements for the Degree

Doctor of Philosophy in Computational Sciences

Dissertation Committee:

Dr. Zachariah Sinkala, Chair

Dr. Wandi Ding

Dr. Rachel Leander

Dr. Preston MacDougall

Dr. John Wallin

This dissertation is dedicated to my father Mr. Edmund M. Ewool, my mother Mrs. Cecilia M. Ewool and my wife Mrs. Lynsey T. Ewool. I am eternally grateful.

ACKNOWLEDGMENTS

I would like to take this opportunity to thank God for helping me throughout my study and to come this far. I want to thank my adviser Dr Zachariah Sinkala for his expert help, patience and fatherly guidance. I could not have completed this dissertation without all your input. I am also very greatful to all the members on my dissertation committee, Drs John Wallin, Preston MacDougall, Wandi Ding and Rachel Leander. Thank you for all the constructive suggestions, criticism and corrections.

I want to express my sincere gratitude to the chairs, Dr Donald Nelson, Dr Marva Lucas and the entire staff of the departments of Mathematics and University Studies for the financial support and the opportunity to teach. I want to thank my colleagues Matthew Wang and Harish Bhatt for all the fruitful discussions.

Finally I will like to say a big thank you to my beautiful wife Lynsey for standing by my side throughout this journey.

ABSTRACT

Angiogenesis is the formation of new blood vessels from pre-existing vessels. It is one of the main processes that help in the growth and spread of tumors. The processes that lead to angiogenesis are very complex and involve several pathways. If cancerous cells are successful in inducing angiogenesis then the harmless malignant tumor cell becomes vascularized and is equipped with the ability to spread from one part of its host to other distant sites. We construct a multiscale continuum model for tumor angiogenesis in an attempt to understand the role of angiogenesis induced by hypoxia (lack of oxygen of tumor cells). We model this process as a reaction diffusion system of a system of semi-linear parabolic differential equations. For modeling blood structures, we use a discrete model which comprises of systems of ordinary differential equations and stochastic differential equations. We use analytic semigroups, functional analysis and complex analysis to study the existence of positive global solutions, linear stability and instabilities due to different diffusion rates (Turing Instability). We perform sensitivity analyis of the reaction system which is modeled using ordinary differential equations and uncertainty quantification via polynomial chaos expansion (the expansions depends on random parameters). For computing the numerical solutions of the continuum model, we use B-spline collocation method. Computations for the numerical methods were done using Python software.

TABLE OF CONTENTS

LIST OF TABLES

LIST OF FIGURES

CHAPTER 1

INTRODUCTION

Tumor-induced angiogenesis is the process by which malignant cancerous cells recruit endothelial cells to ensure their continual survival. This process is complex and involves different pathways. We study angiogenesis in tumor cells that are driven by hypoxia (lack of oxygen). Tumor cells become hypoxic when they no longer have enough nourishment through diffusion from their neighboring environment. To continue survival, tumor cells release signaling factors which constitute the so called angiogenic switch to recruit blood vessels to themselves in order to ensure continuous growth [20].

The resulting vascular network that is formed as a result of tumor induced angiogenesis is leaky due to loose binding of pericytes and exhibits abnormal and irregular branching in the vessel network. The leaky vasculature assists the transportation of cancerous cells to other parts of the body. This process is known as metastasis and can potentially be fatal [3]. We note however that cancer is not the only disease that develops as a result of pathological angiogenesis. Some of the other diseases include, psoriasis, rheumatoid arthritis, macular degeneration due to age and stroke just to mention a few. In 1979 Dr Judah Folkman of MIT children's hospital postulated that, angiogenesis is the main initiator for tumor growth and metastasis [20]. Since then several scientists have been interested in investigating his hypothesis which has over time developed into a big field of research for both experimentalists and modelers.

Advances made by researchers in the field of angiogenesis suggests that biological experiments are insufficient to acquire detailed insights about the intricate dynamics involved in tumor induced angiogenesis. Modelers and experimentalists alike agree

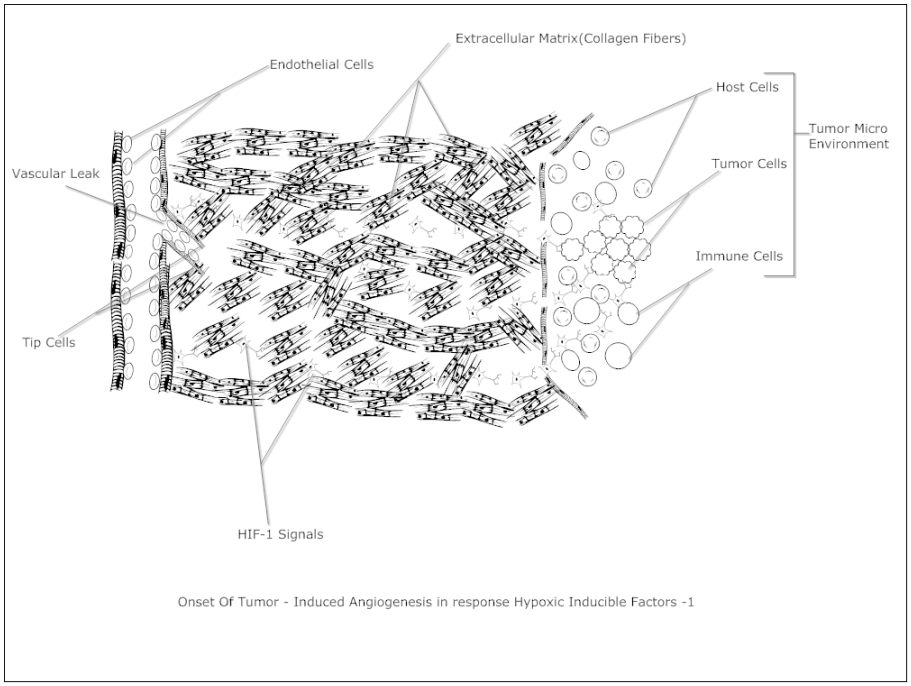

Figure 1: *The following diagram show Hypoxic Inducible Factor -1 (HIF-1) signaling activated as a result of oxygen deficiency in tumor cells. Endothelial cells respond to the hypoxic signals by growing tip cells and moving along the gradient of the signaling factors towards the tumor site.*

that complex time scales restrict experimental design and analysis [12].

The application of mathematical and computational techniques to construct multiscale models for tumor induced angiogenesis has been identified as an alternative approach to the scientific investigation of cancers, by which experimentalist can refine their hypotheses, focus experiments, and generate more accurate predictions. Many researchers [10, 12, 46, 57] have demonstrated the value of this approach in providing quantitative insights in the initiation, progression, and treatment of cancer.

The majority of the recent mathematical cancer models describes the overall behavior of cancers at a single biological time scale [12, 39, 40]. These models do not account for the interactions between processes happening at varying time scales. Due

to recent advancements in computational power it possible to simulate large complex nonlinear systems associated with cancer [57]. Multiscale mathematical cancer modeling involves the construction of models that capture cross-scale effects on the overall behavior of cancer progression. These models have to quantify parameters and establish relationships between biological processes that occur at different scales, the complexity of model design is thus significantly increased.

We propose a multiscale continuum model that describes the effect of hypoxia on pathological angiogenesis in conjunction with a discrete model to capture vascular structure of the blood vessels growing towards the tumor. The continuum model consists of a number balance on the endothelial cells, which is coupled with the set mass balances describing selected factors in the micro-environment : the chemotactic response to tumor angiogenic factors, the haptotactic response of endothelial cells to adhesive gradient and the role of the inhibitors in the angiogenic process. We seek to use mathematical and computational modeling to describe quantitatively the effect that the Hypoxia Inducible Factor-1 has on tumor induced angiogenesis.

We assume the interactions between tumor cells and other cells as a reaction diffusion system. One can describe this relationship by a weakly coupled system of parabolic partial differential equations: Let Ω be a finite domain in $\mathbb{R}^n, n = 1, 2, 3$ and $x \in \mathbb{R}^n$ be spatial coordinate and t denote the time, then the governing equations corresponding to this system are given as

$$\frac{\partial u_i}{\partial t} = d_i \nabla^2 u_i + f_i(u, k), \ i = 1, 2, \cdots, N, \ (0, T) \times \Omega \tag{1}$$

where u is the state vector comprising of cells, (immune cells, host cells, endothelial cells and tumor cells) protein concentration and chemical concentrations. The function f models the interactions between proliferation, apoptosis, dynamics of pro-

duction, uptake and degradation of the chemical components included in the model and k is the vector parameter. In the absence of diffusion equation (1) becomes a reaction equation which is an ordinary differential equation:

$$\frac{du_i}{dt} = f_i(u,k),\ i = 1,2,...,N \tag{2}$$

The state variables $u_i, i = 1,2,\ldots,N$ are non negative. Therefore the reaction equations must preserve positivity, that is $u_i(0) \geq 0$ at $t = 0$ implies $u_i(t) \geq 0$ for all $t \geq 0$. Equation (2) has this property if $f_i(u_1,u_2,\ldots,u_{i-1},0,u_{i+1},\ldots,u_N,k) \geq 0$. This property guarantees global positive solutions for equation (2). The existence of local and global solutions for ordinary differential equations is well covered in the literature [27, 28, 29]. If we add the diffusion terms then the existence of positive global solutions, depends on the quasi-positivity of the nonlinear part of equation (1), which we call condition (P) that is

$$(\mathbf{P}),\ u \in \mathbb{R}^N_+ \rightarrow f_i(u_1,...,u_{i-1},0,u_{i+1},...,u_N,k) \geq 0. \tag{3}$$

and the total mass of the component, must be a priori bounded on all finite $T's$,

$$(\mathbf{M}),\quad \text{For all } u \in \mathbb{R}^N_+,\ \sum_{i=1}^{N} a_i f_i(u_i,k) \leq 0. \tag{4}$$

Condition (M) can be generalized to the following condition;

$$(\mathbf{M}^\star)\ \ \text{for all}\, u \in \mathbb{R}^N_+, \sum_{i=1}^{N} a_i f_i(u_i,k) \leq C\left(1 + \sum_{i=1}^{N} u_i\right) \tag{5}$$

where $C \in [0,\infty)$. Note that when $C = 0$ condition $M(\star)$ becomes M. P and M are sufficient to guarantee global positive solutions if the diffusion rates are equal. For example if $d_i = 0$ in the case of ODEs then P and $M^\star$ guarantees global existence of positive solutions but if the diagonal elements are different, then the different

diffusion rates can cause the loss of stability see [53, 54] and thus the two conditions are insufficient. We need an extra condition to establish the global existence of solutions. We impose an extra condition described as follows:

for all $u \in \mathbb{R}^N_+$

$$Lf(u) \leq \left[1 + \sum_{i=1}^{N} u_i\right] b, \tag{6}$$

where L is a lower triangular invertible matrix with nonnegative entries, b is a constant vector in $\mathbb{R}^N_+$ and the usual order in $\mathbb{R}^N$ is used. For the mathematical analysis (existence of global positive solutions and linear analysis) of equation (1), we use analytic semigroups, functional analysis and complex analysis.

Although the continuum model in equation (1) can provide significant insight into the mechanism of angiogenesis, it cannot predict the vascular structures. We consider next a discrete model for predicting the vascular structures that are formed by sprouts. This model takes into account the existence of separate sprouts from endothelial cells. A very well known model for describing the vascular network is by Stokes and Lauffenburger [59]: In their model, the evolution of the tip velocity is governed by a stochastic differential equation that comprises of viscous damping terms, a white noise term to model motion, and a chemotactic term;

$$dv_i(t) = -\beta v_i(t)dt + \sqrt{\alpha}dW_i(t) + \kappa \nabla a \sin\left(\frac{\Phi}{2}\right) dt \tag{7}$$

where β is the viscosity coefficient, W is the Wiener process, a white noise, a is tumor angiogenic factor concentration, Φ is the angle between the direction the tip is moving and that toward the tumor angiogenic factor source, and i denotes ith sprout. The equation of the tip given by the deterministic equation

$$\frac{dx_i}{dt} = v_i(t); \tag{8}$$

and the equation for average density is

$$\begin{aligned}\frac{d\rho_i}{dt} = k_g\frac{\rho_{\max}-\rho_i(t)}{\rho_{\max}-\rho_{\min}}\rho_i(t) - \frac{s_i(t)}{L_i(t)}\rho_i(t) + k_b\left[\rho_{pv}(t)-\rho_i(t)\right] \\ -\sum_{j=1}^{\nu_i} k_b\left[\rho_i(t)-\rho_j(t)\right]\end{aligned} \tag{9}$$

where k_g is the proliferation rate, k_b is the distribution coefficient, $\rho_{pv}(t)$ is the number of branches that the ith sprout has at time t, s_i in the instantaneous speed of the i th sprout has calculated as $s_i(t) = \|v_i(t)\|$ and L_i is the sprout length calculated from

$$\frac{dL}{dt} = s_i(t). \tag{10}$$

In equation (9), the first term represents the endothelial cell proliferation using a logistic expression, the second term represent sprout elongation using an average velocity and average length, the third term represents the rate of increase of the average density of the ith sprout due to influx of the endothelial cells from the parent vessel, and the fourth term represents the rate of loss of density due to the redistribution of endothelial cells from the ith sprout to its ν_i branches.

In biological systems like angiogenesis, the parameters of the continuum model are not always certain. Thus we need to quantify how uncertainty in the parameters impacts the solutions to the reaction equation model associated with the multiscale tumor induced angiogenesis model with uncertain parameters. We study uncertainty quantification for reaction equation version of our model by using generalized polynomial chaos expansions on the parameters [15]. We use local and global quantitative sensitive analysis methods like elementary local sensitivity analysis and Sobols method to reduce the number of parameters to consider for randomness for uncertainty quantification. We do this because performing uncertainty quantification for a large set of parameters is computationaly costly. Sensitivity analysis also helps us to identify the parameters that have the most effect on the system behavior.

For computing numerical solutions for the multiscale model proposed, we use a Bspline collocation method and generalized polynomoal chaos for uncertainty quantification. We perform all numerical computing using python.

1.1 Dissertation Outline

The dissertation is divided into 7 chapters. In **Chapter 1** we present a general introduction to modeling tumor induced angiogenesis and the various analysis that we will be performed to establish the existence of gloabal positive solutions for the model. **Chapter 2** discusses the construction of the multiscale mathematical models for tumor induced angiogenesis. We review existing models [31, 40, 39] and present the framework of our multiscale model. **Chapter 3** discusses the mathematical analysis for the models we proposed in chapter 2. We discuss the local existence of solutions, and the global existence of positive solutions using conditions, P, $M^\star$ and the extra condition. For the mathematical analysis, we use analytic semigroups, funtional analysis and complex analysis. In **Chapter 4**, we discuss linear analysis of the multiscale model. We present our numerical results for the multiscale model in **Chapter 5** and show the effect of random parameters in the multiscale model in **Chapter 6** and Lastly we conclude by discussing our results in **Chapter 7** and some milestones achieved.

CHAPTER 2

MATHEMATICAL MODELS FOR TUMOR INDUCED ANGIOGENESIS

2.1 A Simplified Continuum Model and its Associated Discrete Model for Angiogenesis

Before we build a multiscale model, we consider in this section a simplified version of the reaction diffusion equation which comprises of two state variables which represent tumor angiogenic factors and inhibitor concentrations. In the model below the inhibiitor specifically binds to and removes TAFs from the system. This tumor angiogenesis model was first proposed by [62] to study the proliferation of tumor angiogenic factors. [31] elaborated on [62] by adding the inhibitor component to study the interaction between tumor angiogenic factors and the inhibitor. In [14] a step function forcing term which depends on a time parameter τ_0 was added to study the effect of a tumor source on the overall dynamics of the system:

$$\begin{aligned} \frac{\partial C}{\partial t} &= D_c \bigtriangledown^2 C + Q(t, \tau_0) - KC - \mu l C - K_{on} IC, \\ \frac{\partial I}{\partial t} &= D_i \bigtriangledown^2 I - K_{on} IC, \end{aligned} \tag{11}$$

with initial conditions,

$$C(x, y, 0) = \begin{cases} 1 & max(|x - x_0|, |y - y_0|) \leq \alpha_0, \\ 0 & \text{otherwise}, \end{cases}$$

$$I(x,y,0) = \begin{cases} 10 & |x-x_0| + |y-y_0| \leq \alpha_1, \\ 0 & \text{otherwise}, \end{cases}$$

where the state variables C and I represent the concentrations for tumor angiogenic factors and inhibitor respectively, D_c and D_i represent the diffusion rate constant for tumor angiogenic factors (TAF) and inhibitors respectively, K, represents the natural inactivation rate of TAFs, μ is the rate constant for the uptake of TAFs, l, denotes local density of cells, K_{on} is the rate constant controlling the relationship between the TAFs and inhibitors. The step function Q is assumed to be a time dependent source term of the form

$$Q(t,\tau_0) = \begin{cases} 0 & \text{if}\,(0 \leq t \leq \tau_0), \\ Q_p & \text{if}\,(t \geq \tau_0), \end{cases}$$

where τ_0 is the time it takes the tumor to initiate new signaling factors, Q_p is the amount of signaling factors introduced after time $t \geq \tau_0$ and α_0, α_1 are fixed positive real numbers. This model gives us some insight into the mechanism of tumor angiogenesis but do not predict the vascular network. To simulate the vascular structures we couple the continuum model (11) with the following discrete model:

$$f(C) = \begin{cases} 0 & \text{if}\, 0 \leq C < C_t, \\ 1 - exp[-\alpha(C - C_t)], & \text{if}\, C_t \leq C, \end{cases}$$

$$f(I) = \begin{cases} 0 & \text{if}\, 0 \leq I < I_t, \\ 1 - exp[-\alpha(I - I_t)], & \text{if}\, I_t \leq I, \end{cases}$$

where C_t and I_t are threshold functions imposed on this model in order to detect when and where endothelial cells can grow or be suppressed. Next the direction of growth which is affected by three main factors namely the endothelial cells previous direction of motion, the TAF concentration gradient and the inhibitor concentration gradient and lastly the rotational matrix which incorporates the possibility of random directions. The equation for the direction of growth is defined as follows:

$$\begin{bmatrix} E_x \\ E_y \end{bmatrix}^T = \left(P \begin{bmatrix} E_x^0 \\ E_y^0 \end{bmatrix}^T + \frac{(1-P)}{2} f(C) \begin{bmatrix} C_x^0 \\ C_y^0 \end{bmatrix}^T - \frac{(1-P)}{2} f(I) \begin{bmatrix} I_x^0 \\ I_y^0 \end{bmatrix}^T \right) \begin{bmatrix} cos\theta & sin\theta \\ -sin\theta & cos\theta \end{bmatrix}, \tag{12}$$

and the length of growth is affected by the maximum velocity of the length increase V_{max} and a time increment Δt which provide the extension of the vascular structure. Its governing equations are defined as;

$$\Delta l = V_{max} \left| f(C) \begin{bmatrix} C_x^0 \\ C_y^0 \end{bmatrix} - f(I) \begin{bmatrix} I_x^0 \\ I_y^0 \end{bmatrix} \right| \Delta t, \tag{13}$$

Detail description of the model together with the associated variables is discribed in [31]. The proof of global positive solutions for equation (11) is not obvious since the diffusion rates are different [53, 54]. However, condition (P) and $(M^\star)$ are satisfied for equation (11) . But they are not enough to guarantee global solutions. In chapter 3 we discuss additional conditions that will make the system (11) have global positive solutions. We simulate the dynamics of the endothelial cell formation in response to TAF which acts as a chemoattractant, see figure (2) and (3).

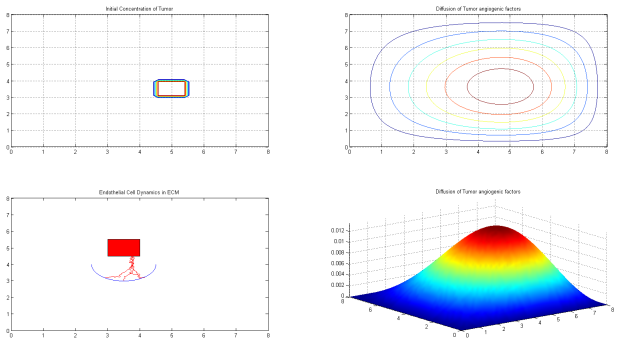

Figure 2: *Simulation describing the effect of TAF spread on the growth of blood vessels resulting in vascularization.*

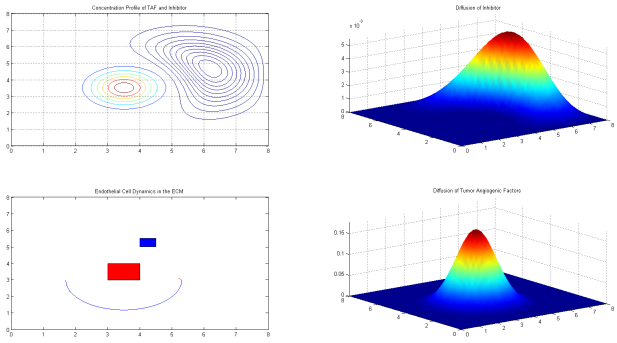

Figure 3: *Simulation describing the effect of the interpaly between TAF and inhibitor on the growth of blood vessels.*

In the next section, we start building the multiscale model by considering first a cancer model for tumor induced angiogenic switch.

2.2 A Cancer Model for Tumor Induced Angiogenic Switch

As a starting point for building a multiscale model, we the impact of cellular interactions in the process of tumor induced angiogenesis as they are described in the model proposed in [39] in order to understand the aggregate contribution and interaction between, host cells, tumor cells, immune cells and endothelial cell on the growth of the tumor. The model proposed by [39] studies the interactions that occur at a single tumor location as diffusion is ignored. The diagram in figure (4) describes the interaction between the various types of cells described at the cellular level.

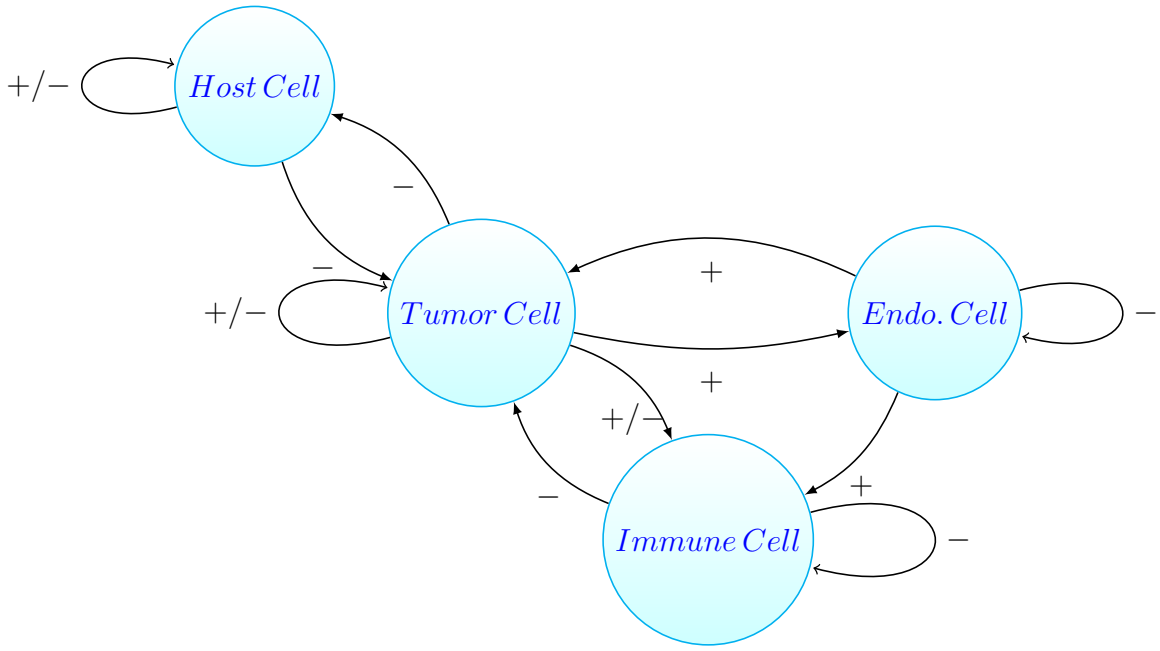

Figure 4: *Flow graph for the interaction between host, tumor, immune and endothelial cells.*

In figure (4) we observe that three main relations take place. The first relation is between tumor and endothelial cells. This relationship is established when the tumor cells become oxygen deficient and require oxygen and other nutrients through endothelial cells to survive. A successful interaction results in the benign tumor

becoming vascularized and metastatic [30]. This describes the so-called angiogenic switch. The second relationship that is established is the one between tumor cells and the immune cells. This occurs because immune cells begin to act in response to abnormal behavior of tumor cells. Tumor cells can respond positively to immune cells by initiating the apoptosis pathway and self destructing or tumor cells are able to secrete chemicals that allow for more production of immune cells. With time the tumor cells are able to develop resistance to the immune cells and thus are able to operate freely irrespective of the presence of the immune cells [63, 56]. The last interaction is between the host cells and the tumor cells which compete for resources within the system.

In [39, 41] the above interaction is described using the laws of mass action and Michealis-Menten kinetics which gives the following system of ordinary differential equation;

$$\begin{aligned}
\frac{dv_1(t)}{dt} &= k_1 v_1(1-v_1) - k_2 v_1 v_3, \\
\frac{dv_2(t)}{dt} &= \frac{k_2 v_2 v_3}{1+v_3} - k_4 v_2 v_3 - k_5 v_2 + k_6 v_2 v_4, \\
\frac{dv_3(t)}{dt} &= k_7 v_3(1-v_3) - k_8 v_3 v_1 - k_9 v_3 v_2 + \frac{k_{10} v_3 v_4}{1+v_4}, \\
\frac{dv_4(t)}{dt} &= \frac{k_{11} v_3 v_4}{1+v_3} - k_{12} v_4,
\end{aligned}$$

where the state variables v_1, v_2, v_3 and v_4 represents the population of host, immune, tumor and endothelial cells respectively, and the parameter values are given in table 1.

In section 2.3, we discuss subcellular interaction associated with apoptosis in the tumor cell.

Table 1: *Parameter values for modeling angiogenic switch model obtained from Louise-Viger [39, 41]*

Parameter	Meaning	Parameter Value
k_1	Host cell growth rate	0.518
k_2	Host cell killing rate by tumor cells	1.500
k_3	Effector immune cell growth rate	4.500
k_4	Effector immune cell inhibition by tumor	0.200
k_5	Effector immune cell natural death rate	0.500
k_6	Simulation of effector immune cell by endo. cells	0.300
k_7	Tumor growth rate	1.000
k_8	Tumor killing rate by host cells	1.000
k_9	Tumor cell killing rate by effector immune cells	2.500
k_{10}	Tumor cell growth rate due to angiogenesis	0.750
k_{11}	Endothelial cell growth rate	0.86
k_{12}	Endothelial cell natural death rate	1./11.0

2.3 A Model of Apoptosis Effect in Tumor Spread

It has been observed that most cancerous cells trigger angiogenesis and metastasize [24, 23] rather than initiate apoptosis. We consider a simplified model proposed by [40] that describes the interplay between angiogenesis and apoptosis within a tumor cell and the various chemical components that are implicated in each process. In figure (5) we consider the two compartmental model describing the pathways for angiogenesis and apoptosis respectively. Oxygen actively participates in the mechanisms in either compartments. The presence of Oxygen inhibits hif-1. In its absence hif-1 binds to P300 which is a co-activator to stimulate the production of vascular endothelial growth factor (a particular type of tumor angiogenic factor) and hence starts the process of angiogenesis which leads to the production endothelial cells. On the other hand the lack of oxygen can also lead p53 to compete with HIF-1 and bind with p300. In addition, p53 directly inhibits $hif-1$ but triggers caspases (casp) which activates cell death. Furthermore, oxygen induced Potassium is a hypothesized in

[40] to inhibit casp.

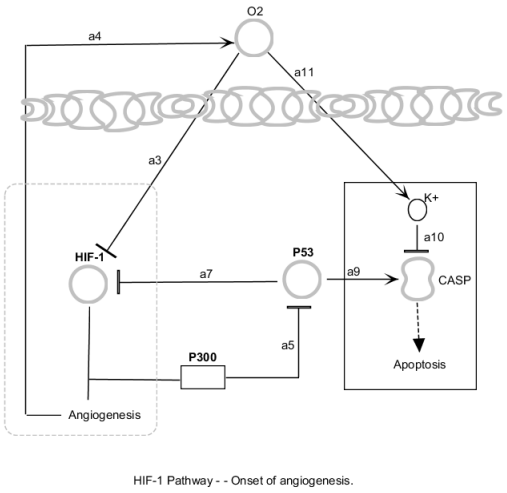

Figure 5: *The schematic diagram for the subcellular angiogenic and apoptotic pathway.*

The resulting model describes the chemical interaction that exists within the two compartments of the apopotic model as shown in figure (5). The chemical equations are given as follows;

$$
\begin{aligned}
O_2 + (HIF-1) &\rightarrow^{a_3} \oslash, \\
(HIF-1) + P300 &\rightarrow^{a_4} O_2, \\
P300 + P53 &\rightarrow^{a_5} \oslash, \\
P53 + (HIF-1) &\rightarrow^{a_7} P53, \\
P53 &\rightarrow^{a_9} CASP, \\
O_2 &\rightarrow^{a_{11}} K^+, \\
CASP &\rightarrow^{a_{13}} \oslash, \\
K^+ &\rightarrow^{a_{14}} \oslash.
\end{aligned}
$$

A more detailed explanation of the model and the chemical interaction is provided in [40] and the references therein. In [40] they used the laws of mass action to obtain the following systems of ordinary differential equations:

$$
\begin{aligned}
\frac{dz_1}{dt} &= a_1 - a_2 z_2 z_1 - a_3 z_1 z_3 - a_4 z_4 z_1, \\
\frac{dz_2}{dt} &= a_5 - a_2 z_2 z_1 + a_3 z_1 z_3 - a_6 z_2, \\
\frac{dz_3}{dt} &= -a_3 z_1 z_3 - a_7 z_3 z_4 + a_8, \\
\frac{dz_4}{dt} &= -a_7 z_4 z_3 + a_9 - a_{10} z_4, \\
\frac{dz_5}{dt} &= a_{10} z_4 - a_{11} z_5 z_6 + a_{12} - a_{13} z_5, \\
\frac{dz_6}{dt} &= -a_{11} z_5 z_6 + a_6 z_2 - a_{14} z_6,
\end{aligned}
$$

where the state variables z_1, z_2, z_3, z_4, z_5 and z_6 represents the concentrations of the hypoxic inducible factor 1(HIF-1), oxygen, P300 co-activator, P53 protein, caspase protease and potassium respectively. The parameter values are given in table 2.

In section 2.4, we construct the multiscale model for tumor induced angiogenesis.

Table 2: *Parameter values for modeling apoptotic effect in tumor spread obtained from Laise [40]*

Parameter	Meaning	Parameter Value
a_1	Rate of production of HIF-1	1.520
a_2	Interaction rate between HIF-1 and O_2	0.900
a_3	Rate of O_2 production due to HIF-1 and P300	0.200
a_4	Rate of P_{53} production due to P_{53} and HIF-1	0.700
a_5	Rate of O_2 production	1.800
a_6	Rate of production K^+ due to O_2	0.200
a_7	Rate of interaction between P300 and P53	0.001
a_8	P300 production rate	0.060
a_9	P53 production rate	0.050
a_{10}	Rate of CASP production due to P53	0.100
a_{11}	Rate of interaction between CASP and K^+	0.700
a_{12}	CASP production rate	0.100
a_{13}	CASP degradation rate	0.100
a_{14}	K^+ production rate	0.050

The multiscale model establishes a connection between cellular and subcellular level interaction.

2.4 A Multiscale Scale Model on the Effect of Apoptosis and the Angiogenic Switch

Having described the angiogenic switch model which is induced largely by hypoxia we want to investigate the effect of hypoxia on the tumor cell proliferation. Since the model for the apoptotic pathways captures the pathway of hypoxia we decided to establish a connection between the two models to understand more clearly the effects of hypoxia. If tumor cells takes the apoptotic pathway, then we assume that there is an interaction between the tumor cells and the Caspases protease. This gives rise to a new term that we include in the tumor model. We observe that this interaction

occurs at some given rate k_{13}. However, if the angiogenic pathway is to be activated, then there exists an interaction between the HIF-1 pathway and the endothelial cells as hypoxia drives the production of endothelial cells. This interaction also occurs at a give rate k_{14}. In addition equation$\dfrac{dv_2(t)}{dt} = \dfrac{k_2 v_2 v_3}{1+v_3} - k_4 v_2 v_3 - k_5 v_2 + k_6 v_2 v_4$, in section 2.3 is replaced by $\dfrac{du_8(t)}{dt} = \dfrac{k_2 u_8 u_9}{1+u_9} - k_4 u_8 u_9 - k_5 u_8 + \dfrac{k_6 u_8 u_{10}}{1+u_{10}}$.
This addition ensures that the overall solution structure is controlled. We can thus formulate a multiscale model from the previous models discussed by establishing a connection between the apoptotic pathway in tumor cells and the HIF-1 pathway effects on endothelial cell production as follows;

$$\begin{aligned}
\frac{du_1(t)}{dt} &= a_1 - a_2 u_2 u_1 - a_3 u_1 u_3 - a_4 u_4 u_1,\\
\frac{du_2(t)}{dt} &= a_5 - a_2 u_2 u_1 + a_3 u_1 u_3 - a_6 u_2,\\
\frac{du_3(t)}{dt} &= -a_3 u_1 u_3 - a_7 u_3 u_4 + a_8,\\
\frac{du_4(t)}{dt} &= -a_7 u_4 u_3 + a_9 - a_{10} u_4,\\
\frac{du_5(t)}{dt} &= a_{10} u_4 - a_{11} u_5 u_6 + a_{12} - a_{13} u_5,\\
\frac{du_6(t)}{dt} &= -a_{11} u_5 u_6 + a_6 u_2 - a_{14} u_6,\\
\frac{du_7(t)}{dt} &= k_1 u_7 (1-u_7) - k_2 u_7 u_9,\\
\frac{du_8(t)}{dt} &= \frac{k_2 u_8 u_9}{1+u_9} - k_4 u_8 u_9 - k_5 u_8 + \frac{k_6 u_8 u_{10}}{1+u_{10}},\\
\frac{du_9(t)}{dt} &= k_7 u_9 (1-u_9) - k_8 u_9 u_7 - k_9 u_9 u_8 + \frac{k_{10} u_9 u_{10}}{1+u_{10}} - k_{13} u_5 u_9,\\
\frac{du_{10}(t)}{dt} &= \frac{k_{11} u_9 u_{10}}{1+u_9} - k_{12} u_{10} + \frac{k_{14} u_1 u_{10}}{1+u_1}.
\end{aligned} \tag{14}$$

The state variables and parameters for the first six equations and last four equations have their usual meaning described in section 2.2 and 2.3 respectively. We estimate the parameters k_{13} and k_{14} using linear regression of the caspases model solution to the caspases data (caspases data obtained from [32]).

One obtains a multiscale reaction diffusion system when diffusion terms are introduced into equation (14) which describes the temporal spatial distribution of the various state variables.

2.5 Spatio-Temporal Models for Tumor Induced Angiogenesis

Adding diffusion terms in a reaction model may give more insight about the systems behavior. A classical example where the addition of diffusion terms gives more details is descibed in [10]. Including the diffusion terms, one obtains the following spatio-temporal multiscale system of partial differential equations defined on a rectangular domain:

$$
\begin{aligned}
\frac{\partial u_1(t)}{\partial t} &= d_1\nabla^2 u_1 + a_1 - a_2u_2u_1 - a_3u_1u_3 - a_4u_4u_1,\\
\frac{\partial u_2(t)}{\partial t} &= d_2\nabla^2 u_2 + a_5 - a_2u_2u_1 + a_3u_1u_3 - a_6u_2,\\
\frac{\partial u_3(t)}{\partial t} &= d_3\nabla^2 u_3 - a_3u_1u_3 - a_7u_3u_4 + a_8,\\
\frac{\partial u_4(t)}{\partial t} &= d_4\nabla^2 u_4 - a_7u_4u_3 + a_9 - a_{10}u_4,\\
\frac{\partial u_5(t)}{\partial t} &= d_5\nabla^2 u_5 + a_{10}u_4 - a_{11}u_5u_6 + a_{12} - a_{13}u_5,\\
\frac{\partial u_6(t)}{\partial t} &= d_6\nabla^2 u_6 - a_{11}u_5u_6 + a_6u_2 - a_{14}u_6,\\
\frac{\partial u_7(t)}{\partial t} &= d_7\nabla^2 u_7 + k_1u_7(1-u_7) - k_2u_7u_9,\\
\frac{\partial u_8(t)}{\partial t} &= d_8\nabla^2 u_8 + \frac{k_2u_8u_9}{1+u_9} - k_4u_8u_9 - k_5u_8 + \frac{k_6u_8u_{10}}{1+u_{10}},\\
\frac{\partial u_9(t)}{\partial t} &= d_9\nabla^2 u_9 + k_7u_9(1-u_9) - k_8u_9u_7 - k_9u_9u_8 + \frac{k_{10}u_9u_{10}}{1+u_{10}} - k_{13}u_5u_9,\\
\frac{\partial u_{10}(t)}{\partial t} &= d_{10}\nabla^2 u_{10} + \frac{k_{11}u_9u_{10}}{1+u_9} - k_{12}u_{10} + k_{14}u_1u_{10},
\end{aligned}
\tag{15}
$$

with Neumann $\left(\frac{\partial u}{\partial n} = 0\right)$ or Dirichlet boundary conditions $u = 0$. With initial conditons

$$u_i(x,0) = \begin{cases} \gamma_0, & \max(|x_i - x_{i0}|, |y_i - y_{i0}|) \\ 0, & otherwise \end{cases}$$

u_{i0} is the initial condition for the reaction terms in the multiscale model. We discuss the existence of global positive solutions and stability of the multiscale model in chapter 3 and 4 respectively. A draw-back of the multiscale reaction diffusion system is that it does not represent the blood vessels distribution in response to tumor angiogenic factors. In order to do this, we use a discrete stochastic equation in predicting the vascular network.

2.6 Discrete Model for Tumor Induced Angiogenesis

Stokes and Lauffenburger used a random diffusion term to control the random movement of the endothelial cell tips instead of the rotation matrix used in [14, 31]. In the discrete model the ith subscript denotes the state of the ith blood vessel sprout. The model is comprised of a deterministic tip equation;

$$\frac{dx_i}{dt} = v_i(t),$$

whiles the movement of the tip velocity is governed by a stochastic differential equation;

$$dv_i(t) = -\beta v_i(t)dt + \sqrt{\alpha}dW_i(t) + \kappa \nabla a \sin\left(\frac{\Phi}{2}\right)dt,$$

where β is the viscosity coefficient, W is the Wiener process, a white noise, a is TAF concentration, Φ is the angle between the direction the tip is moving and that toward

the TAF source, and i denotes ith sprout. Φ is defined more explicitly as

$$\Phi = cos^{-1}\left[\frac{(x_a - x_i)cos\theta_i + (y_a - y_i)sin\theta_i}{((x_a - x_i)^2 + (y_a - y_i)^2)^{1/2}}\right]$$

and finally the equation for the average density is

$$\frac{d\rho_i}{dt} = k_g\frac{\rho_{\max} - \rho_i(t)}{\rho_{\max} - \rho_{\min}}\rho_i(t) - \frac{s_i(t)}{L_i(t)}\rho_i(t) + k_b\left[\rho_{pv}(t) - \rho_i(t)\right] - \sum_{j=1}^{\nu_i} k_b\left[\rho_i(t) - \rho_j(t)\right]$$

where, k_g is the proliferation rate, k_b is the distribution coefficient, $\rho_{pv}(t)$ is the number of branches that the ith sprout has at time t, s_i in the instantaneous speed of the ith sprout has calculated as $s_i(t) = \|v_i(t)\|$ and L_i is the sprout length calculated from

$$\frac{dL_i}{dt} = s_i(t). \tag{16}$$

Table 3: *Parameter values for modeling discrete stochastic differential equation are obtained from Stokes and Lauffenburger [59]*

Parameter	Meaning	Parameter Value
ρ_p	Linear cell number density	10e-4
k_g	Proliferation rate constant	0.02
k_b	Cell redistribution rate constant	0.4
ρ_{max}	Maximum linear cell number density	2.00
ρ_{min}	Minimum linear cell number density	$\rho_{max}/11$
β	Decay rate constant of velocity	1.0/5.5
S	Root mean square speed	40.00
α	Spectrum of white noise	$\beta \cdot S$
κ	Chemotactic responsiveness	0.5
∇a	Attractant gradient	$3.5e-15$

CHAPTER 3

EXISTENCE AND UNIQUENESS OF MULTISCALE REACTION DIFFUSION SYSTEM

3.1 Introduction

We will describe results and tools developed for mathematical analysis of the multiscale reaction diffusion system in section 2.4. This is a system of strongly coupled semi-linear parabolic partial differential equations. We show that this reaction diffusion system satisfy two main natural properties:

(i) Positivity of the solutions is preserved for all time.

(ii) The total mass of the components is controlled for all time.

Condition (ii) suggests that solution should exist for all time. But, it turns out that the answer is not so simple. This explains why so many partial results in different directions are found in the literature on reaction diffusion systems. Thus the general question of global existence of positive solutions is still an open problem.

If we assume there is no diffusion, the multiscale reaction diffusion system becomes a reaction system which can be represented as an ordinary differential equation where $f : [0, \infty)^N \to \mathbb{R}^N$ is a given regular function (representing reaction terms), $u : [0, T) \to \mathbb{R}^N$, and $N = 10$, is the unknown vector function (representing state variables).

$$\dot{u}(t) = f(u), u(0) = u_0 \geq 0. \tag{17}$$

If f satisfies $\sum_{i=1}^{N} f(u_i) \leq 0$ then a local solution exists and may be extended on a maximal interval $[0, T^\star)$ [49, 61].

If f is a quasi-positive ($f_i(u_1, ..., u_{i-1}, 0, u_{i+1}, .., u_N) \geq 0$), $i = 1, 2, \ldots, N$ then $u(t) \geq 0$ for all t [49]. In addition, if we add the system and integrate:

$$\forall\ t,\ \sum_{i=1}^{N} u_i(t) \leq \sum_{i=1}^{N} u_{0_i},$$

together with positivity, then this implies $u(t)$ stays uniformly bounded on $[0, T^\star)$. It follows that $T^\star = +\infty$ and the solution is global [49].

Next if we consider diffusion to occur in the reaction system we get ($N = 10$) reaction diffusion equations, $u = u(t, x)$, $(t, x) \in [0, \infty) \times \Omega$ is the unknown vector function. Let $Q_T = (0, T) \times \Omega$ be a cylinder, where Ω is a bounded open subset of $\mathbb{R}^n$, $n = 1, 2, 3$ and we assume that it has at least a C^2-boundary condition. We write the multiscale reaction diffusion system as follows:

$$\begin{aligned} &u_t = D\Delta u + f(u),\ \text{on}\ Q_T = (0, T) \times \Omega, \\ &\text{Neuman boundary conditions: } \frac{\partial u(t, x)}{\partial \nu} = 0, t > 0, x \in \partial\Omega \\ &\text{Initial conditions: } u(0, x) = u_0(x), x \in \Omega, \end{aligned} \tag{18}$$

where D is an $N \times N$ diagonal matrix with positive diagonal entries. $f : \mathbb{R}^N_+ \to \mathbb{R}^N$ is a $(C^1)^N$-function, u_0 are given.

The positivity condition (**i**) is satisfied if and only if f is quasi-positive which again means that, for $f_i, i = 1, ..., N$;

$$(\mathbf{P}),\ u \in \mathbb{R}^N_+ \to f_i(u_1, ..., u_{i-1}, 0, u_{i+1}, ..., u_N) \geq 0, i = 1, 2, \ldots, N. \tag{19}$$

Condition (**ii**) on the apriori bound of the total mass is satisfied for instance when, for some $a \in \mathbb{R}^N_+$:

$$(\mathbf{M}),\quad \text{For all } u \in \mathbb{R}^N_+,\ \sum_{i=1}^{N} a_i f_i(u_i) \leq 0. \tag{20}$$

To see this in a simple case where the diagonal elements of D are the same, we add up the N equations after multiplying each i-th line by a_i and integrate over $(0,t)\times\Omega$. For these boundary conditions, we will have $-\int_\Omega \triangle u(t,x)dx \geq 0$, so that we obtain the apriori estimate; for all $t \in (0,T), \sum_{i=1}^{N}\int_\Omega a_i u_i(t,x)dx \leq \sum_{i=1}^{N}\int_\Omega a_i u_i(0,x)dx$. If the u_i are initially non-negative then they remain non-negative so that this implies for all $i = 1,...,m, \sup_{t\in(0,T)} \|u_i(t)\|_{L^1(\Omega)} < \infty, \sup_{t\in[0,T]} \sum_{i=1}^{N}\int_\Omega u_i(t,x)dx < \infty$. Then the total mass of the components is uniformly bounded for all time as well as the $L^1(\Omega)$-norm of each component (This means the total mass of the components is uniformly bounded for all $t \in [0,T]$ and $L^1(\Omega)$-norm of each component is uniformly bounded as well for all $t \in [0,T]$). If we replace the property $(\mathbf{M})$ by a more general condition $(\mathbf{M}^\star)$; then for some $C \in [0,\infty)$

$$(\mathbf{M}^\star) \quad \text{for all } u \in \mathbb{R}^N_+, \sum_{i=1}^{N} a_i f_i(u_i) \leq C\left(1 + \sum_{i=1}^{N} u_i\right), \tag{21}$$

condition $(\mathbf{M}^\star)$, gives the same conclusion [50].

We consider next problem (18) as an evolution equation in suitable Banach space $(X = (L^P(\Omega))^N$ or $(C^\alpha(\Omega))^N)$ such that

$$u = U, \quad f(u,k) = F(U,k), \ t \geq 0$$

where U and $F(U)$ are functions belonging to a suitable Banach space or subspace of X. The choice of X depends on what results we are expecting, or on the regularity of the initial condition data. We write equation (18) as an abstract Cauchy problem:

$$\begin{aligned} &U_t = -AU + F(U,k), t \geq 0, \\ &\text{Initial conditions: } U(0) = u_0, \end{aligned} \tag{22}$$

where $A = -D\triangle u$, $D(A) = \{u \in X : \frac{\partial u}{\partial n} = 0\}$. Our main interest is to study the well-posedness of the Cauchy problem (22). That is we seek for a suitable Banach

space X such that $-A$ generates an analytic semigroup in X and then show that the Cauchy problem (22) or its integral form

$$u = e^{-tA}u_0 + \int_0^t e^{-(t-s)A}F(u)\,ds, \tag{23}$$

generates a strong continuous flow in X. In particular, for any $u_0 \in X$ there exist a time interval $I = [0, T)$ and a unique function $u(t) \in C(I; X)$ satisfying (23). The case $T < \infty$ and for $T = \infty$ correspond to the local and global well-posedness respectively. The solution in the function space of X of the integral equation (23) is usually defined as the mild solution of the Cauchy problem (22). We note in addition that, since mild solutions are differentiable with respect to time, t, they are thus strong solutions of the problem (22) due to the regularity of the analytic semigroup e^{-At}. The $(L^p(\Omega))^N$ theory or $(C^\alpha(\Omega))^N, \alpha \geq 0$, theory together with the bootstrap method implies that the mild solution u of the problem (22) is also a classical solution [47]. The theory of ordinary differential equations is not easily extendible to these type of problems. The main obstacle is that the linear operator A is defined on a proper subspace of X, and it is not continuous.

We need a spectral property of A in order for us to define the solution of the following equation:

$$\begin{aligned} &U_t = -AU,\ t \geq 0, \\ &U(0) = u_0. \end{aligned} \tag{24}$$

Let us denote the solution of the homogeneous equation (24) by $e^{-tA}u_0$. We use the following spectral property of A to define the solution $e^{-tA}u_0$: the resolvent set of A contains a sector $S = \{\lambda \in \mathbb{C} : \lambda \neq 0,\ |\arg\lambda| < \theta\}$, with $\frac{\pi}{2} < \theta < \pi$ and moreover

$$\|(\lambda I - A)^{-1}\|_{\mathcal{L}(X)} \leq \frac{M}{|\lambda|}, \lambda \in S. \tag{25}$$

If A satisfies the spectral property we say that A is sectorial operator [26]. $\mathcal{L}(X)$ is a set of all linear bounded operators form X into X. Just like in ordinary differential

equations, in general the solution of equation (22) is defined only in small time interval $[0, T]$. The problem of global existence of a positive solution of equation (22) applies to the multiscale reaction diffusion system in section 2.4 of chapter 2. We give sufficient conditions for global existence of positive solutions.

The theory of analytic semigroups is a tool for studying parabolic partial differential equations, in particular the multiscale reaction diffusion systems. Yosida is one of the main contributors to analytic semigroups [38]. Since Yosida's contributions, the analytic semigroups have attracted great attention by researchers working on the foundations of the theory, as well as by researchers working on applied problems. Analytic semigroups have proved to be applicable to a wide array of partial differential equations which have a parabolic structure, typically reflecting the fact that the processes they model are irreversible in time. The range of applicability includes problems in areas as diverse as physics, biology, chemistry, ecology, medicine, fluid dynamics, free boundary problems, phase transitions, material sciences, and geometric evolutions laws, to mention only a few.

3.2 Preliminaries and Definitions

In this section, we state the preliminaries on linear operators in Banach space and calculus for Banach space valued functions defined on a real interval. The preliminaries are assumed to be either known to the reader or extend easily from finite dimensional theory;

Definition 3.1 *The family of operators* $\{e^{tA} : t \geq 0\}$ *is an analytic semigroup, if it satisfies*

$$e^{(t+s)A} = e^{tA}e^{sA},\ t, s \geq 0,\ e^{0A} = I,$$

and the function $(0,\infty) \to \mathcal{L}(X),\ t \to e^{tA}$ *is analytic.*

Definition 3.2 *A linear operator* $A : D(A) \subset X \to X$ *is sectorial if there are constants* $\omega \in \mathbb{R}$, $\frac{\pi}{2} < \theta < \pi$, $M > 0$ *such that*

(i) The resolvent set of A *contains a sector* $S_{\theta,\omega} = \{\lambda \in \mathbb{C} : \lambda \neq \omega,\ |\arg \lambda - \omega| < \theta\}$,

(ii)

$$\|R(\lambda, A)\| = \|(\lambda I - A)^{-1}\|_{\mathcal{L}(X)} \leq \frac{M}{|\lambda - \omega|}, \lambda \in S_{\theta,\omega}. \tag{26}$$

For every $t > 0$, the two conditions in Definition (3.2) make us to define a bounded linear operator e^{tA} on X, through an integral formula. Let $r > 0, \eta \in (\pi/2, \theta)$, and the curve

$$\gamma_{r,\eta} = \{\ \lambda \in \mathbb{C} : |\arg \lambda| = \eta,\ |\lambda| \geq r\} \cup \{\lambda \in \mathbb{C} : |\arg \lambda| \leq \eta,\ |\lambda| = r,\ \}$$

oriented counterclockwise. For each, $t > 0$ we set

$$e^{tA} = \frac{1}{2\pi i} \int_{\gamma_r, \eta+\omega} e^{t\lambda} R(\lambda, A) d\lambda,\ t > 0. \tag{27}$$

Lemma 3.3 *If* A *is a sectorial operator then the integral in (27) is well defined, and it is independent of* $r > 0$ *and* $\eta \in (\pi/2, \theta)$.

Theorem 3.4 *Let* A *be a sectorial operator and let* e^{tA} *be represented by integral (27). Then, the following statements are true:*

(i) $e^{tA}x \in D(A^k)$ *for all* $t > 0, x \in X, k \in \mathbb{N}$ *and if* $x \in D(A^k)$, *then*

$$A^k e^{tA} = e^{tA} A^k,\ t \geq 0,$$

(ii) $e^{tA} e^{sA} = e^{(t+s)A}$ *for any* $t, s \geq 0$.

(iii) There exist constants $M_0, M_1, M_2, ..,$ *such that*

(a)

$$\|e^{tA}\|_{\mathcal{L}(X)} \leq M_0 e^{\omega t},\ t > 0,$$

(b)

$$\|t^k(A-\omega)e^{tA}\|_{\mathcal{L}(X)} \leq M_k e^{\omega t},\ t > 0,$$

where ω *is the real number in Definition 3.2. In particular, (iii) (b) implies that for every* $\epsilon > 0$ *and* $k \in \mathbb{K}$ *there is* $C_{k,\epsilon} > 0$ *such that*

$$\|t^k(A^k e^{tA})\|_{\mathcal{L}(X)} \leq C_{k,\epsilon} e^{(\omega+\epsilon)t},\ t > 0. \tag{28}$$

(iv) The function $t \to e^{tA}$ *belongs to* $C^\infty((0,\infty); \mathcal{L}(X))$*, and the equality*

$$\frac{d^k e^{tA}}{dt^k} = A^k e^{tA}, t > 0, \tag{29}$$

holds for every $k \in \mathbb{N}$*.*

Statement (ii) in Theorem 3.4 tells us that the family of operators e^{tA} satisfies the semigroup law, an algebraic property which is coherent with the exponential notation. Statement (iv) tells us that e^{At} is analytically extendable to a sector by analytic continuation. Therefore, it is natural to give the following definition.

Definition 3.5 *If* A *is a sectorial operator. The function* $e^{-tA} : [0, +\infty) \mapsto \mathcal{L}(X)$ *is called the analytic semigroup generated by* A *(in* X*).*

Coming back to the Cauchy problem (24), one notice that Theorem 3.4 implies that the function

$$u(t) = e^{-tA}x,\ t \geq 0$$

is analytic, with values in $D(A)$ for $t > 0$, and by (iv) it is a solution of the differential equation in (24), for $t > 0$. Moreover, u is continuous also at $t = 0$ ($u(t) \in X$) if and only if $x \in \overline{D(A)}$ and in this case u is a solution of the Cauchy problem (24). If $x \in D(A)$ and $Ax \in \overline{D(A)}$, then u is continuously differentiable up to $t = 0$, and it satisfies the differential equation also at $t = 0$, i.e., $u'(0) = Ax$. The proof of uniqueness of the solution, $u(t) = e^{-tA}x_0$, to (24) uses Gronwal inequality.

Suppose $\{e^{-tA} : t \geq 0\}$ is an analytic semigroup of bounded linear operators on X. Also, let F be an X-valued mapping on $D(F) \subset [0, +\infty) \times X$ that is continuous with respect to some fractional power of A. We will investigate the existence of solutions and determination of invariants sets for the Cauchy problem (22). We will study (22) indirectly by studying the following integral equation that is obtained from (22) by variation of constants:

$$U(t) = e^{-tA}u_0 + \int_0^t e^{-(t-s)A}F(U(s), k)ds, \ t \geq 0. \tag{30}$$

3.3 The Multiscale Reaction Diffusion System has Properties P and M or M*

We show that the multiscale reaction diffusion systems satisfies properties (**P**) and (**M**) or (**M***). To show condition (P) we proceed as follows;

$$\begin{array}{ll} f_1(0, \ldots, u_{10}) = a_1 > 0, & f_6(u_1, \ldots, 0) = a_6u_2 > 0, \\ f_2(u_1, 0, \ldots, u_{10}) = a_5 + a_3u_1u_3 > 0, & f_7(u_1, \ldots, u_7, \ldots, u_{10}) = 0, \\ f_3(u_1, u_2, 0, \ldots, u_{10}) = a_8 > 0, & f_8(u_1, \ldots, 0, \ldots, u_{10}) = 0, \\ f_4(u_1, u_2, u_3, 0, \ldots, u_{10}) = a_9 > 0 & f_9(u_1, \ldots, u_9, u_{10}) = 0, \\ f_5(u_1, \ldots, 0, u_{10}) = a_{10}u_4 + a_{12} >, 0 & f_{10}(u_1, \ldots, u_{10}) = 0. \end{array} \tag{31}$$

since $f_i(u_1, 0, u_3, \ldots, u_{10}) \geq 0$ for $i = 1, \cdots 10$ then f is quasi-positive. Thus condition (P) is satisfied.

Next we check condition $(M^\star)$ for the multiscale reaction diffusion system.

Let $u = (u_1, u_2, u_3, u_4, u_5, u_6, u_7, u_8, u_9, u_{10})$ then the reaction terms for the multiscale model is given as

$$\begin{aligned}
f_1(u) &= a_1 - a_2u_2u_1 - a_3u_1u_3 - a_4u_4u_1,\\
f_2(u) &= a_5 - a_2u_2u_1 + a_3u_1u_3 - a_6u_2,\\
f_3(u) &= -a_3u_1u_3 - a_7u_3u_4 + a_8,\\
f_4(u) &= -a_7u_4u_3 + a_9 - a_{10}u_4,\\
f_5(u) &= a_{10}u_4 - a_{11}u_5u_6 + a_{12} - a_{13}u_5,\\
f_6(u) &= -a_{11}u_5u_6 + a_6u_2 - a_{14}u_6,\\
f_7(u) &= k_1u_7(1-u_7) - k_2u_7u_9,\\
f_8(u) &= \frac{k_2u_8u_9}{1+u_9} - k_4u_8u_9 - k_5u_8 + \frac{k_6u_8u_{10}}{1+u_{10}},\\
f_9(u) &= k_7u_9(1-u_9) - k_8u_9u_7 - k_9u_9u_8 + \frac{k_{10}u_9u_{10}}{1+u_{10}} - k_{13}u_5u_9,\\
f_{10}(u) &= \frac{k_{11}u_9u_{10}}{1+u_9} - k_{12}u_{10} + \frac{k_{14}u_1u_{10}}{1+u_1},
\end{aligned}$$

since

$$f_1 + f_2 + \cdots + f_{10} \le a_1 + a_5 + a_8 + a_9 + a_{12} + a_{10}u_4 + k_1u_7 + k_2u_8 + k_6u_8 +$$

$$k_7u_9 + k_{11}u_{10} + k_{14}u_1 + k_{10}u_9.$$

Let $A = a_1 + a_5 + a_8 + a_9 + a_{12}$, $k^\star = \max(k_1, k_2, k_6, k_7, k_{11}, k_{10})$, such that $A^\star = \max(A, K^\star)$then

$$\begin{aligned}
f_1 + f_2 + \cdots + f_{10} &\le A + \sum_i k^\star u_i,\ i = 1, 2, 4, 7, 8, 9, 10\\
&\le A^\star + \sum_{i=1}^{N} A^\star u_i,\\
&= A^\star(1 + \sum_{i=1}^{N} u_i).
\end{aligned}$$

Since $A^\star$ is nonnegative and $A^\star \in [0,\infty)$, it implies that the multiscale reaction diffusion system satisfies the condition $(M^\star)$.

3.4 Local Existence and Uniqueness Using Semigroups

Lemma 3.6 *Let $u_0 \in (L^\infty(\Omega))^N$. Then, there exists $T > 0$ and a unique classical solution to the multiscale system on $[0,T]$. If $T^\star$ denotes the supremum of all these $T's$ and*

$$\sup_{t\in[0,T^\star]} \left(\sum_{i=1}^{N} \|u_i(t)\|_{L^\infty(\Omega)} \right) < +\infty \text{ then } T^\star = +\infty \tag{32}$$

Furthermore, if the nonlinearity f is quasi-positive then

$$u_0 \geq 0 \text{ implies that } u(t) \geq 0, \text{ for all } t$$

Proof: The proof follows easily from [50]. For ordinary differential equations, the local existence result is proved via a Banach fixed-point argument.

In the case of parital differential equations, we proceed as follows; We choose an adequate ball B subset of $C(Q_T, \mathbb{R}^N)$ under the $L^\infty(Q_T)$-norm and we consider the mapping $\hat{u} \in B \to u \in B$ which takes $\hat{u}$ to the solution of the following initial-boundary value problem;

$$\frac{\partial u}{\partial t} - D\triangle u = f(\hat{u}) \text{ on } Q_T,$$

$$\frac{\partial u}{\partial \nu} = 0 \text{ (or } u = 0) \text{ on } (0,T)\times\partial\Omega,$$

$$u(0) = u_0,$$

which we rewrite using variational constant formula as

$$u(t) = e^{-At}u_0(x) + \int_0^t e^{-A(t-s)} f(\hat{u}(x,t))dt,$$

where $A = D\triangle u$, $D(A) = \{u \in (L^\infty(\Omega))^N : \frac{\partial u}{\partial t}, \triangle u \in C(\Omega)\}$. Thus by the locally Lipschitz property of f, this is a strict contraction if T is small enough. Hence the existence of a solution on $[0, T]$ and on a maximal interval $[0, T^\star)$. The solution to the variational form is a mild solution to the reaction diffusion equation. If $u \in D(A)$ then u is a classiscal solution of the reaction diffusion equation. The characterization (32) follows from the fact that $T^\star$ depends only on the L^∞-norm of the initial data. Finally, the solution obtained in this way is regular since $\{e^{-At}, t \geq 0\}$ is analytic semigroup. Note that any weak solution with values in $L^\infty(Q_T)$ is actually regular enough to be a classical solution, and it is even C^∞ in the interior of Q_T if f is itself C^∞. Using (32), in order to prove global existence of classical solutions for the multiscale model, it is sufficient to prove that if $T^\star < +\infty$ then the solutions u are uniformly bounded on $[0, T^\star)$. Thus, a priori L^∞-bounds imply global existence.

If all the diffusion coefficients are equal in any reaction diffusion system (for all $i = 1, ..., N, d_i = d$) then

$$\frac{\partial \left(\sum_{i=1}^N a_i u_i\right)}{\partial t} - d\triangle \left(\sum_{i=1}^N a_i u_i\right) \leq 0,$$

by maximum principle, we get

$$\text{for all } t \in [0, T^\star),\ \| \sum_{i=1}^N a_i u_i(t)\|_{L^\infty(\Omega)} \leq \| \sum_{i=1}^N a_i u_{0i}\|_{L^\infty},$$

combining positivity, this implies a uniform L^∞ bound on each $u_i(t)$,

thus $T^\star = +\infty$. The situation is quite more complicated if the diffusion coefficients are different from each other. We need an extra condition to guarantee global solutions.

3.5 Global Existence of Classical Solutions

Theorem 3.7 *If $f \in C^1\left([0,\infty)^N, \mathbb{R}^N\right)$ is at most polynomial growth and satisfies the quasi-positivity condition* $(\mathbf{P})$ *and there exist $b \in \mathbb{R}^N$ and a lower triangular invertible $N \times N$ matrix L with nonnegative entries such that for all $u \in \mathbb{R}^N_+$*

$$Lf(u) \leq \left[1 + \sum_{i=1}^{N} u_i\right] b, \tag{33}$$

where the usual order in $\mathbb{R}^N$ is used. Then the systems

$$\begin{aligned} &u_t = D\Delta u + f(u), \text{ on } Q_T = (0,T) \times \Omega, \\ &\frac{\partial u}{\partial \nu} = 0 \left(\text{ or } u = 0 \right), \text{ on } (0,T) \times \partial\Omega, \\ &u(0,.) = u_0 \in L^\infty(\Omega), \ u_0 \geq 0, \end{aligned} \tag{34}$$

has positive global solutions.

We show that the reaction terms for the multiscale model satisfy equation (33) of theorem (3.7) by constructing the associated lower triangular matrix L and vector b as follows;

$$\begin{aligned} f_1(u) &\leq a_1 := A_1, \\ &\leq \left(1 + \sum_{i=1}^{N} u_i\right) A_1, \\ f_1(u) + f_2(u) &\leq A_1 + a_5 := A_2, \\ &\leq \left(1 + \sum_{i=1}^{N} u_i\right) A_2, \\ f_1(u) + f_2 + f_3(u) &\leq A_2 + a_8 := A_3 \\ &\leq \left(1 + \sum_{i=1}^{N} u_i\right) A_3, \\ f_1(u) + \cdots + f_4(u) &\leq A_3 + a_9 := A_4, \\ &\leq \left(1 + \sum_{i=1}^{N} u_i\right) A_4 \end{aligned}$$

$$
\begin{aligned}
f_1(u) + \cdots + f_5(u) &\leq A_4 + a_{12} + a_{10} := A_5, \\
&\leq (1 + u_4)\, A_5 \\
&\leq \left(1 + \sum_{i=1}^{N} u_i\right) A_5 \\
f_1(u) + \cdots + f_6(u) &\leq A_5 + a_6 := A_6, \\
&\leq (1 + u_2)\, A_6 \\
&\leq \left(1 + \sum_{i=1}^{N} u_i\right) A_6, \\
f_1(u) + \cdots + f_7(u) &\leq A_6 + k_1 := A_7, \\
&\leq (1 + u_7)\, A_7, \\
&\leq \left(1 + \sum_{i=1}^{N} u_i\right) A_7, \\
f_1(u) + \cdots + f_8(u) &\leq A_7 + (k_2 + k_6) := A_8, \\
&\leq \left(1 + \sum_{i=1}^{N} u_i\right) A_8 \\
f_1(u) + \cdots + f_9(u) &\leq A_8 + (k_7 + k_{10}) := A_9, \\
&\leq (1 + u_9)\, A_9, \\
&\leq \left(1 + \sum_{i=1}^{N} u_i\right) A_9 \\
f_1(u) + \cdots + f_{10}(u) &\leq A_9 + (k_{11} + k_{14}) := A_{10}, \\
&\leq (1 + u_{10})\, A_{10} \\
&\leq \left(1 + \sum_{i=1}^{N} u_i\right) A_{10}
\end{aligned}
$$

Thus we obtain the following lower triangular matrix L, for the reaction terms associated with the multiscale model as

$$L = \begin{bmatrix} 1.0 & 0 & 0 & 0 & 0 & 0 & 0 & 0 & 0 & 0 \\ 1.0 & 1.0 & 0 & 0 & 0 & 0 & 0 & 0 & 0 & 0 \\ 1.0 & 1.0 & 1.0 & 0 & 0 & 0 & 0 & 0 & 0 & 0 \\ 1.0 & 1.0 & 1.0 & 1.0 & 0 & 0 & 0 & 0 & 0 & 0 \\ 1.0 & 1.0 & 1.0 & 1.0 & 1.0 & 0 & 0 & 0 & 0 & 0 \\ 1.0 & 1.0 & 1.0 & 1.0 & 1.0 & 1.0 & 0 & 0 & 0 & 0 \\ 1.0 & 1.0 & 1.0 & 1.0 & 1.0 & 1.0 & 1.0 & 0 & 0 & 0 \\ 1.0 & 1.0 & 1.0 & 1.0 & 1.0 & 1.0 & 1.0 & 1.0 & 0 & 0 \\ 1.0 & 1.0 & 1.0 & 1.0 & 1.0 & 1.0 & 1.0 & 1.0 & 1.0 & 0 \\ 1.0 & 1.0 & 1.0 & 1.0 & 1.0 & 1.0 & 1.0 & 1.0 & 1.0 & 1.0 \end{bmatrix}$$

and the vector b as

$$b = \begin{bmatrix} A_1 \\ A_2 \\ A_3 \\ A_4 \\ A_5 \\ A_6 \\ A_7 \\ A_8 \\ A_9 \\ A_{10} \end{bmatrix}$$

such that $Lf(u) \leq (1 + \sum_{i=1}^{10} u_i)b$. The remaining part of the proof follows from Pierre [50].

The multiscale model satisfy theorem (3.7) and therefore, there exist global positive solutions for the multiscale model described in equation (14).

CHAPTER 4

LINEAR ANALYSIS

4.1 Introduction

In this chapter, we give conditions for the multiscale reaction diffusion system (14) to exhibit diffusion driven instability (Turing Instability) at steady state. We assume all the hypothesis of chapter 3 so that global positive solution u exists and is uniformly bounded for initial data in $L^\infty(\Omega)$. In the next section we state the necessary definitions and results on stability.

4.2 Stability

In this chapter, the ultimate fate of the system is our main focus, that is asymptotic state as time goes to infinity. Let $u^* \equiv u^*(x)$ be a uniform steady-state solution of the multiscale reaction diffusion system (14). For Dirichlet boundary conditions, uniform steady states of (14) are possible if and only if $u^\star = 0$. Moreover, a uniform steady state $u^\star$ are stable against uniform perturbations, if and only if $u^\star$ is a stable state of the homogeneous system:

$$\frac{du}{dt} = f(u, k).$$

We define the Helmholtz operator: $\mathcal{H} = -D\triangle + I$ such that for $\alpha \geq 0$ we let the fractional powers of $\mathcal{H}$ be defined as $\mathcal{H}^\alpha$. The domain of $\mathcal{H}^\alpha$, $\mathcal{D}(\mathcal{H}^\alpha)$ is equipped with the graph norm $\|\cdot\|^\alpha_{D(H)} = \|\cdot\|_p + \|\mathcal{H}^\alpha\|_p$ is continuously embedded in $C(\Omega)$ equipped with the sup norm, provided $\alpha > 0$ [37].

Definition 4.8 *The uniform state $u^\star(x) \equiv u^\star$ is Lyapunov stable if for any $\epsilon >$*

0, *there exist* $\delta > 0$ *such that any solution* u *with* $\|u_0 - u^*\|_{D(H^\alpha)^N} < \delta$ *satisfies* $\|u(t) - u^*\|_{D(H^\alpha)^N} < \epsilon$ *for all* $t > 0$.

Definition 4.9 *The uniform steady state* $u^\star(x) \equiv u^\star$ *is asymptotically stable in the sense of Lyapunov if there exist* $\delta > 0$ *such that if* $\|u_0 - u^*\|_{D(H^\alpha)^N} < \delta$ *then*

$$\|u(t) - u^*\|_{D(H^\alpha)^N} \to 0, \text{ as } t \to \infty.$$

u^* *is said to be unstable if it is not stable.* u^* *is globally asymptotically stable if every solution of (14) converges to* $u^\star(x) \equiv u^\star$

Now we consider linearization about a spatially homogeneous steady state. Let $w(t) = u(t) - u^\star$. The evolution of perturbation of $w(t)$ is

$$\frac{dw}{dt} = Jw + Q(w)$$

where J is the Jacobian of f, evaluated at $u^\star$

$$Q(w) = o(w), \text{ as, } w \to 0.$$

$$\|Q(w) - Q(v)\|_{(L^2)^N} \leq h(\rho)\|w - v\|_{D(H^\alpha)^N} \text{ for } \|w\|_{D(H^\alpha)^N} \leq \rho, \tag{35}$$

for some function $h : \mathbb{R}_+ \to \mathbb{R}_+$, continuous in 0 with $h(0) = 0$. By subtracting Bw on both sides we obtain an equation for the perturbed solution w,

$$\partial_t w + Lw = Q(w), \tag{36}$$

where $L = D\triangle - B$. If $w(t) \equiv 0$ is an asymptotically stable solution of the linearized system

$$\partial_t w - D\triangle w = Bw, \tag{37}$$

then we say that u^* is linearly stable. If the intersection $\sigma(L) \cap \{\lambda \in \mathbb{C} | Re\lambda < 0\}$ is non-empty where $\sigma(L)$ is the spectrum of L, then we say that u^* is linearly unstable.

Lemma (4.10) is essential in proving theorem (4.11).

Lemma 4.10 *Let $\{e^{-At}, t \geq 0\}$ be an analytic semigroup generated by a sectorial operator $-A$ and let $\delta \geq 0$ be such that $-A+\delta$ generates an analytic semigroup. The following properties then hold for the semigroup e^{-At} and the fractional powers of A:*

1. *$e^{-At} : (L^p(\Omega))^N \to D(A^\alpha)$ for all $t > 0$,*
2. *$\|e^{-At}\|_{D(A^\alpha)} \leq C_{\alpha,p} t^{-\alpha} \exp(-\delta t)\|u\|_p$ for all $t > 0$, $u \in (L^p(\Omega))^N$,*
3. *$e^{-tA} A^\alpha u = A^\alpha e^{-At} u$ for all $t > 0$, $u \in D(H^\alpha)$.*

Proof: It follows directly from Theorem 6.13 in [26]

Theorem 4.11 *1. If u^* is linearly stable then u^* is asymptotically stable;*

2. If u^* is linearly unstable then u^* is unstable.

Proof Since L is a sectorial operator ([26] section 1.3) then it generates an analytical semigroup $\{e^{-Lt}, t \geq 0\}$. Let $\eta > 0$ be such that $Re\lambda > \eta$ whenever $\lambda \in \sigma(L)$. By lemma 4.10 there exist $\Phi \geq 1$ such that

$$\|e^{-Lt} w\|_{D(H^\alpha)^N} \leq \Phi \exp(-\eta t)\|w\|_{D(H^\alpha)^N}, \Phi t^{-\alpha} \exp(-\eta t)\|w\|_{(L^2(\Omega))^N}.$$

By inequality (35), $\rho > 0$ so that

$$h(\rho)\Phi \int_0^\infty \xi^{-\alpha} \exp(-(\eta - s)\,\xi)\; d\xi < \frac{1}{2},$$

$$\|Q(w)\|_{(L^2)^N} \leq h(\rho)\|w\|_{D(H^\alpha)^N}, \text{ for } \|w\|_{D(H^\alpha)^N} \leq \rho,$$

where $0 < s < \eta$

Let $\|w(0)\|_{D(H^\alpha)} \leq \dfrac{\rho}{2\Phi}$. Then by continuity of the solution $\|w(t)\|_{D(H^\alpha)^N} \leq \rho$ on some time interval and therefore by variation of constants:

$$\begin{aligned}
\|w(t)\|_{D(H^\alpha)^N} &\leq \Phi \exp(-\eta t)\|w(0)\|_{D(H^\alpha)^N} \\
&+ h(\rho)\Phi \int_0^t (t-\tau)^{-\alpha} \exp(-\eta(t-\tau))\|w(\tau)\|_{D(H^\alpha)^N} d\tau, \\
&\leq \frac{\rho}{2} + h(\rho)\Phi \int_0^t (t-\tau)^{-\alpha} \exp(-\eta(t-\tau)) d\tau < \rho.
\end{aligned}$$

Therefore,

$$\|w(t)\|_{D(H^\alpha)^N} < h(\rho). \tag{38}$$

By continuity, either $\|w(t)\|_{D(H^\alpha)^N} < \rho$ for all $t > 0$ or $\|w(t)\|_{D(H^\alpha)^N} = \rho$ at some finite time t. The second case is not possible since it contradicts the sharp inequality (38). Thus $\|w(t)\|_{D(H^\alpha)^N} < \rho$ for all $t > 0$.

Let

$$\Theta(t) = \sup_{0 \leq \xi \leq t} \|w(\xi)\|_{D(H^\alpha)^N} \exp(s\xi),\ t \geq 0.$$

By inequality (38), we get

$$\begin{aligned}
\|w(\xi)\|_{D(H^\alpha)^N} \exp(s\xi) &\leq \Phi \exp(-(\eta - s)t)\|w(0)\|_{D(H^\alpha)^N} \\
&+ h(\rho)\Phi \int_0^\xi (\xi-\tau)^{-\alpha} \exp(-\eta(t-\tau)) d\tau \times \Theta(\xi), \\
&\leq \frac{\rho}{2} + \frac{1}{2}\Theta(t),
\end{aligned}$$

for all $0 \leq \xi \leq t$ and thus

$$\Theta(t) \leq \frac{\rho}{2} + \frac{1}{2}\Theta(t).$$

and $\Theta(t) \leq \rho$ and hence

$$\|w(t)\|_{D(H^\alpha)^N} \leq \rho \exp(-st).$$

This shows that u^* is asymptotically stable. Hence part 1 of the theorem is true.

Next we prove part 2. We show that there exist $\epsilon > 0$ and a sequence $\{u_0^{(n)}\}_{n=1}^{\infty} \in (L^2(\Omega))^N$ such that $\sup_{t\geq 0} \|u_n(t) - u^*\|_{D(H^\alpha)^N} \geq \epsilon > 0$, where u_n are the solutions corresponding to the initial data u_0^n. Let $0 \notin \sigma(L)$. If $0 \in \sigma(L)$ then by assumption, there exist $\beta > 0$ such that the spectrum is disjoint from the ball in $\mathbb{C}$ with center 0 and radius 2β. Note that we assume the eigenvalues of the operator L are real. Let $\sigma_1 = \sigma(L) \cap \{\lambda \in \mathbb{C} | Re\lambda < 0\}$ and $\sigma_2 = \sigma(L) \setminus \sigma_1$, where σ_1 is a set of finite numbers in $\mathbb{C}$.

We diagonalize

$$\sum_{n=1}^{\infty} \lambda_n \langle w, w_n \rangle_{(L^2)^N} w_n,$$

as follows:

we decompose the set $\mathcal{J}$ into $(N-1)$ disjoint subsets $\mathcal{J}_i$ as follows;

$$\mathcal{J}_i = \{i\}, i = 1, 2, \ldots, N-2,$$

and

$$\mathcal{J}_{N-1} = \{N-1, \ldots, J\}.$$

We set

$$X_i = span\{w_n : n \in \mathcal{J}_i\},\ i = 1, 2, \ldots, N-1$$

and

$$X_N = \overline{span\{w_n : n \in \{J+1, J+2, \ldots\}\}}.$$

such that

$$(L^2(\Omega))^N = X_1 \oplus X_2 \oplus \cdots \oplus X_N$$

For each projection operator onto X_i is denoted by $P_i,\ i = 1, \ldots, N$.

Now, let L_i be a restriction of L to X_i, $i = 1, 2, \ldots, N-1$ then L_i is finite dimensional,

and therefore bounded and generates an analytical semigroup $e^{L_i t}$, so that there exist χ_1^i and χ_2^i, such that for $t \leq 0$:

$$\|e^{L_i t}\|_{D(H^\alpha)^N} \leq \chi_1^i \exp(-\beta t)\|P_N w\|_2,\ \chi_2^i t^{-\alpha}\exp(-\beta t)\|P_N w\|_{D(H^\alpha)^N} \text{ for } t > 0,$$

$i = 1, 2, \ldots, N-1$.

Let $\chi = \max\{\chi_1^i, \chi_2^i, i = 1, 2, \ldots N-1\}$.

We claim that $E(t)$ given by the expression:

$$E(t) = \left(\sum_{i=n}^{N-1} \sigma_i e^{-L_i(t-\xi)} + \int_\xi^t e^{L_i(t-\tau)} P_i Q(E(\tau))\right) + \int_{-\infty}^t e^{-L_N(t-\tau)} P_N Q(E(\tau)), \quad (39)$$

solves the semi-linear parabolic reaction diffusion equation for $\sigma_i \in X_i$ and $t < \xi$, $i = 1, \ldots, N-1$. To prove the claim we define the operator T by

$$TE(t) = \left(\sum_{i=n}^{N-1} e^{-L_i(t-\xi)\sigma_i} + \int_\xi^t e^{-L_i(t-\tau)} P_i Q(E(\tau))d\tau\right) + \int_{-\infty}^t e^{-L_N(t-\tau)} P_N Q(E(\tau))d\tau,$$

It follows that T maps

$$B_\rho(0) = \{w \in (C((0,\infty); D(H^\alpha)))^N |\ \|w\|_{D(H^\alpha)^N} \leq \rho, \}$$

where $C(0,\infty)$ is equipped with the norm

$$\|u\|_\infty = \sup_\Omega \|u\|,\ \|u\| = \max_{1\leq i\leq N} |u_i|, \quad (40)$$

$\rho > 0$ is such that

$$\chi^k(\rho)\left(\sum_{i=1}^{N-1}\left(\frac{1}{2}\beta^{-1}\|P_i\|\right) + \|P_N\|\int_0^\infty s^{-\alpha}\exp(-\beta s)ds\right) \leq \frac{1}{4\chi},$$

maps into itself. The following computation, then shows that T is a contraction on $B_\rho(0)$:

$$
\begin{aligned}
\|T\Psi - TE(t)\|_{D(H^\alpha)^N} &\leq \left|\sum_{i=1}^{N-1} \chi^k(\rho)\exp(2\beta(t-\tau))\|P_i\|\|\Psi(\tau)-E(\tau)\|_{D(H^\alpha)^N}\right| \\
&+ \int_{-\infty}^{t} \chi^k(\rho)\exp(-\beta(t-\tau))(t-\tau)^{-\alpha}\|P_N\| \\
&\times \|\Psi(\tau)-E(\tau)\|_{D(H^\alpha)^N}d\tau, \\
&\leq \chi^k(\rho)\sum_{i=1}^{N-1}\|P_i\|\left|\int_{\xi}^{t}\exp(2\beta(t-\tau))d\tau\right| \\
&+ \chi^k(\rho)\|P_N\|\int_{-\infty}^{t}(t-\tau)^{-\alpha}\exp(-\beta(t-\tau))d\tau \\
&\times \sup_{t\leq\xi}\|\Psi(t)-E(t)\|_{D(H^\alpha)^N}, \\
&< \frac{1}{2}\times\sup_{t\leq\xi}\|\Psi(t)-E(t)\|_{D(H^\alpha)^N},
\end{aligned}
$$

by choice ρ, and for Ψ, $E \in B_\rho(0)$. Hence, by Banach's Fixed Point Theorem there is a unique fix point in $B_\rho(0)$. To show that E is a solution of equation (36), we consider the projections of E onto $X_i, i = 1, \ldots, N$. First

$$
\begin{aligned}
P_iE(t) &= e^{-L_i(t-\xi)}\sigma_i + \int_{\xi}^{t} e^{-L_i(t-\tau)}P_iQ(E(\tau))d\tau \\
&= e^{-L_i(t)}e^{-L_i(-s)}\sigma_i + e^{-L_i(t)}\int_{\xi}^{0} e^{L_i(-\xi)}P_iQ(E(\tau))d\tau \\
&+ \int_{0}^{t} e^{-L_i(t-\tau)}P_iQ(E(\tau))d\tau, \text{ for } 0\leq t\leq\xi,\ i=1,\ldots,N-1,
\end{aligned}
$$

and similarly

$$
\begin{aligned}
P_NE &= e^{-L_N(t)}\int_{-\infty}^{0} e^{-L_N(t-\tau)}P_NQ(E(\tau))d\tau \\
&+ \int_{0}^{t} e^{-L_N(t-\tau)}P_NQ(E(\tau))d\tau, \text{ for } 0\leq t\leq\xi,
\end{aligned}
$$

hence

$$\begin{aligned} E(t) &= \sum_{i=1}^{N} P_i(E(t)) \\ &= \sum_{i=1}^{N} e^{-L(t)} \left(e^{-L_i(-\xi)}\sigma_i + \int_{\xi}^{0} e^{-L_i(-s)} P_i Q E(\tau) \right) \\ &+ \int_{-\infty}^{0} e^{L_N(t-\tau)} P_N Q(E(\tau)) d\tau \\ &+ \int_{0}^{t} e^{-L_N(t-\tau)} Q E(\tau) d\tau \\ &= e^{-L(t)} E(0) + \int_{0}^{t} e^{-L(t-\tau)} Q E(\tau)) d\tau, \text{ for } 0 \le t \le \xi, \end{aligned}$$

where

$$e^{L} w = \sum_{i=1}^{N} e^{L_i} P_i w.$$

Thus we conclude that E is the solution of equation (36) with

$$w(0) = E(0).$$

Next, we show that $\|E(t)\|_{D(H^\alpha)^N} \le 2\chi \|\sigma\|_{D(H^\alpha)^N} \exp(2\beta(t-\xi))$ for $t \le \xi$. From equation (39):

$$\begin{aligned} \|E\|_{D(H^\alpha)^N} &\le \chi \exp(2\beta(t-\xi)) \|\sigma\|_{D(H^\alpha)^N} \\ &+ \chi^k(\rho) \left(\left(\sum_{i=1}^{N-1} \frac{1}{2\beta} \|P_i\| \right) + \|P_N\| \int_0^\infty \xi^{-\alpha} \exp(-\beta\xi)\, d\xi \right) \\ &\times \sup_{0 \le s \le \xi} \|E(\tau)\|_{D(H^\alpha)^N}, \ \forall\ t \le \xi \end{aligned}$$

but then

$$\sup_{0 \le s \le \xi} \|E(\tau)\|_{D(H^\alpha)^N} \le \chi \exp(2\beta(t-\xi)) \|\sigma\|_{D(H^\alpha)^N},$$

therefore,

$$\|E(t)\|_{D(H^\alpha)^N} \le \sup_{0 \le s \le \xi} \|E(\tau)\|_{D(H^\alpha)^N} \le 2\chi \exp(2\beta(t-\xi)) \|\sigma\|_{D(H^\alpha)^N}, \ \forall t \le \xi. \quad (41)$$

Now we are ready for the final estimate. By equation (39) we obtain:

$$\begin{aligned}\|E(\xi)-\sigma\| &\leq \int_{-\infty}^{\xi}\chi(\xi-s)^{-\alpha}\exp(-\beta(\xi-s))\|P_N\| \\ &\times \ 2\chi\exp(2\beta(\xi-s))\|\sigma\|_{D(H^\alpha)^N}d\tau, \\ &= \ 2\chi^2\|P_N\|\|\sigma\|_{D(H^\alpha)^N}\int_{-\infty}^{\xi}(\xi-s)^{-\alpha}\exp(-3\beta(t-\tau))d\tau,\end{aligned}$$

then by inequality (40)

$$\|E(\xi)-\sigma\| \leq \frac{1}{2}\|\sigma\|_{D(H^\alpha)^N}, \tag{42}$$

But then, $\|E(\xi)\|_{D(H^\alpha)^N} \geq \frac{1}{2}\|\sigma\|_{D(H^\alpha)^N}$.

The theorem now follows, since if we choose $\|\sigma\|_{D(H^\alpha)^N} \leq \frac{1}{2}$ and $\xi = n$ then by equation (41)

$$\|w(0)\|_{D(H^\alpha)^N} = \|E(0)\|_{D(H^\alpha)^N} \leq \rho\exp(-2\beta n) \to 0, \text{ for } n \to \infty,$$

while

$$\sup_{0\leq t\leq n}\|w(t)\|_{D(H^\alpha)^N} \geq \|w(n)\|_{D(H^\alpha)^N} \geq \frac{1}{2}\|\sigma\|_{D(H^\alpha)^N}, \ \forall\ n \in N,$$

and therefore u^* is unstable [37]. □

Theorem (4.11) tells us that linear stability is a sufficient condition for stability of the nonlinear system. We used this in the next section to state the sufficient conditions for the general autonomous system to exhibit diffusion instability.

4.3 Sufficient Conditions for Diffusion Driven Instability

One of the factors that influence diffusion driven instabilities is the diameter of Ω of the reaction diffusion equation. We transform x and t to $\tilde{x}$ and $\tilde{t}$ using the following transformations; $x = \gamma^{\frac{1}{2}}\tilde{x}$ and $t = \gamma\tilde{t}$, where γ is a fixed parameter. Then using the

new variables the system is transformed into ;

$$\begin{array}{lcl} u_{\tilde{t}} - D\tilde{\triangle}u & = & \gamma f(u) \text{ in } \tilde{\Omega} \times (0,\infty) \\ \dfrac{\partial u}{\partial \tilde{\nu}} & = & 0 \text{ on } \partial\tilde{\Omega} \times [0,\infty) \\ u & = & u_0 \text{ on } \tilde{\Omega} \times \{t=0\} \end{array} \tag{43}$$

where $\tilde{\Omega} = \{x \in \mathbb{R}^n | \gamma^{-1/2} x \in \Omega,\ n = 1,2,3\}$. We can vary γ to study the effect that the diameter of Ω has on the solution. Suppose $u^* \in \mathbb{R}^N_+$ such that $f(u^*) = 0$. We denote $f^\star = f(u^\star)$. For convenience we omit the tilde notation on the transformed system Then we write the Jacobian matrix as;

$$B = \left(\frac{\partial f^\star}{\partial r} \right). \tag{44}$$

Next we define diffusion driven instability;

Definition 4.12 *If the following two conditions*

1. *u^* is asymptotically stable in the absence of diffusion,*

2. *u^* is unstable in the presence of diffusion,*

are met, then the autonomous reaction-diffusion model is said to have diffusion driven instabilities.

We first give sufficient conditions which guarantees condition (1) above.

Theorem 4.13 *All roots of the characteristic polynomial $P(\lambda) = \det(\lambda I - B) = 0$ have negative real parts iff $\triangle_l = \begin{vmatrix} c_1 & c_3 & \dots & \\ 1 & c_2 & c_4 & \dots \\ 0 & 1 & c_2 & \vdots \\ \vdots & \dots & \dots & \vdots \\ 0 & 0 & \dots & c_l \end{vmatrix} > 0, l = 1, \dots, N$ together with condition $c_n > 0$.*

The linearized version of (43) becomes

$$\partial_t w - D\triangle w = \gamma B w, \tag{45}$$

If we ignore the diffusion term in equation (43) then

$$\partial_t w = \gamma B w, \tag{46}$$

where

$$w = u - u^*.$$

The ordinary differential equation in (45) is asymptotically stable if the eigenvalues of γB have negative real part. We can calculate for the eigenvalues by solving

$$\det(\lambda I - B) = 0.$$

$$Re(\lambda) < 0 \text{ if and only if Hurwitz determinants are all positive} \tag{47}$$

Therefore condition 1 in definition (4.12) is satisfied. To verify condition 2 in the definition (4.12), we consider the linear system of equation (37) and determine the condition for linear instability and then summarize using theorem (4.11).

It is well know in literature that the solution, $w(x,t)$, to the system (4.11) can be written as

$$w(x,t) = \sum_{i=1}^{\infty} c_{k_i} \exp(\lambda_{k_i} t) X_{k_i}(x), \tag{48}$$

where $\{c_{k_i}\}$ depend on the initial condition and X_{k_i} are the eigenfunctions of the Laplacian:

$$-\triangle X_{ki} = k_i^2 X_{k_i} \text{ in } \Omega, \tag{49}$$
$$\frac{\partial}{\partial \nu}(X)_{k_i} = 0, \text{ on } \partial\Omega,$$

$u^\star$ is linearly unstable if and only if $Re(\lambda_{k_i}) > 0$ for some $i \in \{1, 2, 3, \ldots.\}$

It is well known that k_i's are real, and we can write them as follows $0 \leq k_1^2 \leq \cdots <$

$k_i^2 \leq \ldots$, and $k_i^2 \to +\infty$ for $i \to \infty$.

Inserting $C_{k_i} \exp(\lambda_{k_i} t) X_{k_i}(x)$ into equation (45) we get

$$\left(\lambda_{k_i} I - \gamma B + k_i^2 D\right) X_{k_i} = 0, \ i = 1, 2, 3, \ldots.$$

To obtain non-trivial solutions, the coefficient matrix must be singular which means

$$\det\left(\lambda_{k_i} I - (\gamma B - k_i^2 D)\right) = 0$$

In other words, this is a characteristic polynomial, associated with a matrix $\gamma B - k_i^2 D$ for each i We find that λ_{k_i} which determines stability of the uniform steady state to infinitesimal perturbation of the form X_i are the eigenvalues of matrix $\hat{B}(k_i^2) = (\gamma B - k_i^2 D)$. The eigenvalues are the roots of the characteristic polynomial $\det\left(\lambda_{k_i} I - (\gamma B - k_i^2 D)\right) = 0$.

Corollary 4.14 *If the following conditions are satisfied:*

1. *all Hurwitz determinants of the characteristic polynomial* $\det(\lambda I - B) = 0$ *are all positive.*

2. *If* $c_N = 0$. *There exist a positive* γ_{T} *such that* $\gamma = \gamma_{\mathrm{T}}$, *for some* J. $\lambda(k_J^2) = 0$. *For* $\gamma < \gamma_{\mathrm{T}}$ $u^\star$ *is stable, while for* $\gamma > \gamma_{\mathrm{T}}$ *then the multiscale reaction-diffusion system exhibits diffusion-driven instabilities at* $u^\star$.

The corollary (4.14) is telling us the following: A Turing instability occurs when for the first time a single real λ_{k_i}, for some nonzero k, passes through a controlled parameter γ is varied, while the real part of all other eigenvalues of $\hat{B}(k_i^2)$ remains negative. That is, as the control parameter is changed, the uniform steady state of the multiscale reaction diffusion becomes unstable at $\gamma = \gamma_T$ to perturbations with a nonzero wave number k_T and the spatial mode $X_{k_T}(x)$ grows into a stationary

spatially nonuniform solution of the multiscale model beyond the Turing threshold γ_T (time independent concentration pattern). The final pattern is determined by the nonlinear terms of the kinetic rate functions and can differ qualitatively from the unstable Turing mode $X_{k_T}(x)$.

CHAPTER 5

NUMERICAL SOLUTIONS FOR TUMOR INDUCED ANGIOGENESIS MODELS

5.1 Introduction Numerical Methods

Numerical methods are used as a means for finding solutions to differential equations which do not have closed form solutions or whose solutions may be difficult to solve using known techniques. To obtain a solution for an ordinary or partial differential equation using a numerical approach, we replace the continuum function with a discretization over a finite space. This transformation results normally in a discrete problem which is solvable over some finite set. Many techniques for solving such discrete problems are available [45, 36]. These methods are known collectively as numerical methods for differential equations. The function $\bar{x}(t)$ is a numerical solution of the differential equation $\dot{x}$ if $\bar{x}$ satisfies the differential equation and makes the residual small. That is the difference between the actual solution $\dot{x}$ and the approximate solution $\bar{x}$ is small enough in the framework of weighted residuals. We can write $\bar{x}$ as a linear combination of some basis function $\phi_j(t)$ such that

$$\bar{x}(t) = \sum_{j=0}^{N} \tilde{x}_j \phi_j(t).$$

Numerical method can thus be classified, based on the trial functions ϕ_j. We call the numerical methods that arises from choosing trial functions of overlapping local polynomials of low order as finite difference methods. If the trial functions are local smooth functions (polynomials of fixed degree which are non-zero only on sub domain on which the function is defined), then the numerical method is known as the Finite

element method and lastly if the trial functions are global smooth functions such as Fourier series or B-splines then we call the numerical method Spectral numerical method. In our research we will be using spectral method with B-splines as our trial functions. One reason why we decided to use bslpines is that they have compact support. For example consider the following ODE model by Bock

$$x_1^{'}(t) = x_2(t), \tag{50}$$

$$x_2^{'}(t) = \mu^2 x_1(t) - (\mu^2 + \rho^2) sin(\rho t), \tag{51}$$

with initial conditions $x_1(0) = 0$ and $x_2(0) = \pi$ and $t \in [0, 1]$.

This system when using numerical integrators to solve can lead to wrong solutions due to error propagation and sometimes due to the stability of the methods being used.However using B-spline collocation method we obtain a good approximation to the solution to (50) We show with several numerical examples using integrators from Python and Matlab to illustrate this bottle neck.

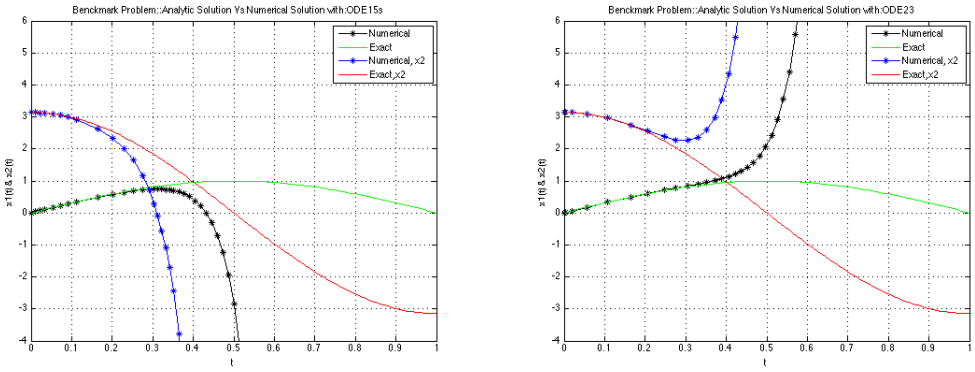

Figure 6: *Solutions to equation (50) using various Matlab solvers. The solvers do not yield correct approximate results due to instabilities.*

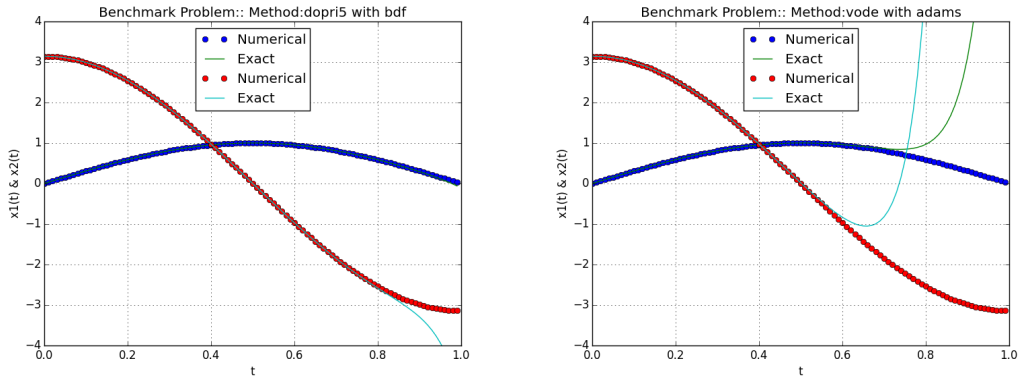

Figure 7: *Solution to equation (50) using various Python solvers. The solvers do not give accurate approximation to the solution due to possible instabilities.*

If one is not careful with how the solutions to the differential equations are being approximated, a black box solver could lead to false results. We thus implemented our technique for approximating the differential equation using B-spline collocation method.

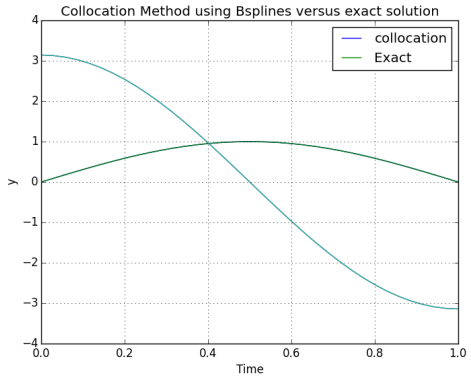

Figure 8: *Solution to equation (50) using Bspline Collocation Method. This method gives an exact approximation to the analytic solution.*

5.1.1 Preliminaries and Definition for B-Spline Collocation Method

Definition 5.15 *A spline function is a piecewise polynomial of order k (the polynomial degree is $k-1$ at most) defined on the interval $\Lambda =]a,b[$, whose high order derivatives possess jump-discontinuities at some breakpoints $\xi = \{\xi_i i = 1, \cdots, l+1\}$ defined by*

$$a = \xi_1 < \xi_2 < \cdots < \xi_i < \cdots < \xi_l < \xi_{l+1} = b, \tag{52}$$

In our work, we will restrict our characterization to splines having jump-discontinuities at their $m+1$ derivatives at each $\xi_i \in \Lambda$, that is splines belonging to the space $C^m(\Lambda)$. The spline $u(x)$ is commonly described in its B-representation as

$$u(x) = \sum_{i=1}^{N} \alpha_i B_i^k(x), \tag{53}$$

where $B_i^k(x)$ is a special spline function of order k called the B-Spline which has, in particular, the property of having compact support. The number N of the B-splines, depending on the order k and the index of regularity m, will be defined in the ensuing sections. Next we shall define explicitly the function $B_i^k(x)$, for $k = 1$

$$B_i^1(x) = \begin{cases} 1 & if\, x \in [\xi_i, \xi_{i+1}], \\ 0 & otherwise, \end{cases}$$

and an efficient construction of the B-Spline of order $k > 1$ is given by the recurrence relation [13, 8]

$$B_i^k(x) = \frac{x - t_i}{t_{i+k-1} - t_i} B_i^{k-1}(x) + \frac{t_{i+k} - x}{t_{i+k} - t_{i+1}} B_{i+1}^{k-1}(x), \tag{54}$$

where

- t_i − knots ie $t_i, i = 1, \cdots, N+k$,

- N $-$ the number of B-splines ie $N = l(k - m - 1) + m + 1$,
- $l-$ the number of intervals between knots,
- m - index of regularity or smoothness of the B-spline,

The regularity of the B-spline basis is imposed through the definition of the knots by requiring

$$t_{k+(i-2)(k-m-1)+1} = \cdots = t_{k+(i-1)(k-m-1} = \xi_i \ for \ i = 2, \cdots, l \tag{55}$$

The construction of the basis leaves freedom in the first k and last k of the knots. A convenient choice for the approximation of the boundary value problem is to set

$$t_1 = \cdots = t_k = a, \ \ t_{N+1} = \cdots = t_{N=k} = b, \tag{56}$$

5.2 Example of B-spline Construction for Ordinary and Partial Differential Equations

In this section we will show how to construct the B-spline basis matrix and its derivative and use it to solve a few examples. Suppose we want to approximate an ordinary differential equation using cubic B-splines and t-collocation points then we will need to derive the B-spline functions together with their derivatives from either the general recursive formula given as:

$$B_i^k(x) = \frac{x - t_i}{t_{i+k-1} - t_i} B_i^{k-1}(x) + \frac{t_{i+k} - x}{t_{i+k} - t_{i+1}} B_{i+1}^{k-1}(x), \tag{57}$$

or an explicit cubic B-spline formula [48]:

$$B_i(t) = \frac{1}{h^3}\begin{cases} (t - s_{i-2})^3, & if\, t \in [s_{i-2}, s_{i-1}] \\ h^3 + 3h^2(t - s_{i-1}) + 3h(t - s_{i-1})^2 - 3(t - s_{i-1})^3, & if\, t \in [s_{i-1}, s_i] \\ h^3 + 3h^2(s_{i+1} - t) + 3h(s_{i+1} - t)^2 - 3(s_{i+1} - t)^3, & if\, t \in [s_i, s_{i+1}] \\ (s_{i+2} - t)^3, & if\, t \in [s_{i+1}, s_{i+2}] \\ 0 & otherwise \end{cases}$$

whose first derivative is given as,

$$B_i^{'}(t) = \frac{1}{h^3}\begin{cases} 3(t - s_{i-2})^2, & if\, t \in [s_{i-2}, s_{i-1}] \\ 3h^2 + 6h(t - s_{i-1}) - 9(t - s_{i-1})^2, & if\, t \in [s_{i-1}, s_i] \\ -3h^2 - 6h(s_{i+1} - t) - 9(s_{i+1} - t)^2, & if\, t \in [s_i, s_{i+1}] \\ -3(s_{i+2} - t)^2, & if\, t \in [s_{i+1}, s_{i+2}] \\ 0 & otherwise \end{cases}$$

higher order derivatives if required can be taken in a similar way. Suppose we want to solve the following Initial value problem $y^{'} - 2y = 0$ when $y(0) = 2$ where $t \in \{0, 2\}$ using 5 B-splines and however many collocation points. Then to generate the number of B-splines we first have to define our knot vector over the the interval where the solution is to be found as follows;

$$[\, s_0 = 0\, s_1 = 0\, s_2 = 0\, s_3 = 0\, s_4 = 1\, s_5 = 2\, s_6 = 2\, s_7 = 2\, s_8 = 2\,]$$

note that the number of additional 0 and 2's at the end of the points is due to the order of the B-spline. When using a cubic B-spline we add 3 zeros and 3 twos at the

ends respectively and this has a knot vector as defined above.

Having created our knot vector we can begin the process of finding our 5 B-spline by iterating through the explicit B-spline function. If we do that we can see that we obtain our first B-spline when $i = 2$, that is;

$$B_1(t) = \frac{1}{h^3}\begin{cases}(1-t)^3, & if\, t \in\ [0,1] \\ \\ 0, & otherwise\end{cases}$$

if we make an increment of $i = 3$ we obtain our next B-spline as follows:

$$B_2(t) = \frac{1}{h^3}\begin{cases}h^3 + 3h^2(1-t) + 3h(1-t)^2 - 3(1-t)^3, & if\, t \in\ [0,1] \\ \\ (2-t)^3, & if\, t \in\ [1,2] \\ \\ 0. & otherwise\end{cases}$$

Following the same process we can obtain all our 5 B-splines and subsequently their derivatives. For example the derivatives of the first and second B-splines will be given as follows

$$B_1^{'}(t) = \frac{1}{h^3}\begin{cases}-3(1-t)^2, & if\, t \in\ [0,1] \\ \\ 0, & otherwise\end{cases}$$

and

$$B_2^{'}(t) = \frac{1}{h^3}\begin{cases}-3h^2 - 6h(1-t) + 9(1-t)^2, & if\, t \in\ [0,1] \\ \\ -3(2-t)^2, & if\, t \in\ [1,2] \\ \\ 0. & otherwise\end{cases}$$

We are now in a position of construct our Basis matrix and derivative of the basis matrix as follows: Recall that the cubic B-spline approximation to a function is given

as;

$$y(t) = \sum_{i=0}^{N-1} c_i B_i^3(t). \tag{58}$$

Thus we can form our system of equations for three collocation points as follows (we choose three collocation points for illustrative purpose only)

$$y(t) = c_0 B_0^3(t) + c_1 B_1^3(t) + c_2 B_2^3(t) + c_3 B_3^3(t) + c_4 B_4^3(t) \tag{59}$$

Thus for $t = 0\,, 1\,, 2$

$$\begin{aligned}
y(0) &= c_0 B_0^3(0) + c_1 B_1^3(0) + c_2 B_2^3(0) + c_3 B_3^3(0) + c_4 B_4^3(0) \\
y(1) &= c_0 B_0^3(1) + c_1 B_1^3(1) + c_2 B_2^3(1) + c_3 B_3^3(1) + c_4 B_4^3(1) \\
y(2) &= c_0 B_0^3(2) + c_1 B_1^3(2) + c_2 B_2^3(2) + c_3 B_3^3(2) + c_4 B_4^3(2)
\end{aligned}$$

We can derive our Basis matrix from the above system of equations and proceed to find our derivative matrix and the solution for the given initial value problem.

$$B_i^3(t) = \begin{pmatrix} B_0^3(0) & B_1^3(0) & B_2^3(0) & B_3^3(0) & B_4^3(0) \\ B_0^3(1) & B_1^3(1) & B_2^3(1) & B_3^3(1) & B_4^3(1) \\ B_0^3(2) & B_1^3(2) & B_2^3(2) & B_3^3(2) & B_4^3(2) \end{pmatrix} \tag{60}$$

Similarly we obtain the $B_i^{'}(t)$ matrix as follows

$$B_i^{3'}(t) = \begin{pmatrix} B_0^3(0) & B_1^{3'}(0) & B_2^{3'}(0) & B_3^{3'}(0) & B_4^{3'}(0) \\ B_0^{3'}(1) & B_1^{3'}(1) & B_2^{3'}(1) & B_3^{3'}(1) & B_4^{3'}(1) \\ B_0^{3'}(2) & B_1^{3'}(2) & B_2^{3'}(2) & B_3^{3'}(2) & B_4^{3'}(2) \end{pmatrix} \tag{61}$$

The system can then be solved for the coefficients c and thus we can find the approximate solution for the function. For the example given above we can find the solution as follows;

$$B_i^{3'}(t) - 2B_i^3(t) = 0 \tag{62}$$

We can apply the initial condition to obtain the appropriate right hand side and solve for the B-spline coefficients, c. Finally we can find our B-spline approximation to the

solution, as

$$y(t) = \sum_{i=0}^{N-1} c_i B_i^3(t). \tag{63}$$

5.3 Computational Algorithm for B-spline Collocation Method: Ordinary Differential Equations

To compute approximate solutions to the ordinary differential equation for initial and boundary value problems using B-spline collocation method, we use the following algorithm:

Algorithm 5.1: B-spline Collocation Method for ODEs.

- 1. Create your Basis matrix using the following information: knot vector, degree of B-spline, collocation points
- 2. Create the nth derivative Basis matrix depending on the order of your ode.
- 3. Create the approximation matrix, V and make sure the necessary conditions are met.
- 4. Construct the right-hand side vector and make sure the first row of the approximation matrix is set appropriately, if its an initial value problem else if its a boundary value problem then set the last row of V appropriately as well. Since the initial and or boundary condition is known.
- 5. Since the approximation matrix V is not normally square multiply V by its transpose on both sides of system
- 6. Solve for coefficients of the B-spline, c

- 7. Approximate solution to the ordinary differntial eqation is $y = Bc$.

5.4 Nonlinear B-spline Collocation Method for Ordinary Differential Equations

Algorithm for solving nonlinear B-spline with polynomial type nonlinearity, is slightly different from the general algorithm 6.1. The initial steps for creating the basis and differential matrices are the same and so we will skip those in this algorithm. We proceed as follows:

Algorithm 5.2: B-spline Collocation Method for Non-linear ODEs.

- 1. Define the right hand side equation as a function.
- 2. Take the tensor product of the differential matrix and the identity matrix. The size of the identity matrix depends on the number of equations.
- 3. Set V appropriately for the initial conditions ie that make substitutions appropriately if we know the initial conditions.
- 4. Setup the initial guess vector using the information from the initial conditions.
- 5. Create the nonlinear function to find residue
- 6. Check condition of matrix. If ill conditioned resolve this issue with singular value decomposition (SVD) of the ill conditioned matrix.
- 7. Using the Newton Krylov nonlinear solver in python we evaluate for the solution of the coefficients.

- 8. Write the B-spline form of the approximation to the function and graph results.

We demonstarte the above procedure described in the algorithm (6.2) with the tumor angiogenesis model on apoptosis and its effect on tumor spread discussed in chapter 2. Consider the systems of reaction equations

$$\begin{aligned}
\frac{dy_1}{dt} &= a_1 - a_2 y_2 y_1 - a_3 y_1 y_3 - a_4 y_4 y_1, \\
\frac{dy_2}{dt} &= a_5 - a_2 y_2 y_1 + a_3 y_1 y_3 - a_6 y_2, \\
\frac{dy_3}{dt} &= -a_3 y_1 y_3 - a_7 y_3 y_4 + a_8, \\
\frac{dy_4}{dt} &= -a_7 y_4 y_3 + a_9 - a_{10} y_4, \\
\frac{dy_5}{dt} &= a_{10} y_4 - a_{11} y_5 y_6 + a_{12} - a_{13} y_5, \\
\frac{dy_6}{dt} &= -a_{11} y_5 y_6 + a_6 y_2 - a_{14} y_6,
\end{aligned}$$

where the state variables y_1, y_2, y_3, y_4, y_5 and y_6 represents the concentrations of the hypoxic inducible factor 1(HIF-1), oxygen, P300 coactivator, P53 protein, caspase protease and potassium respectively. The parameter values are given in table 2. We obtained the following results using the B-spline collocation method discussed in algorithm 5.2

In the next subsection we discuss the numerical results for the system of reaction equations in the multiscale model constructed in chapter 2.

5.4.1 Numerical Results for A Multiscale Model for Tumor Induced Angiogenesis

In this subsection we solve the resulting system of reaction equations for the multiscale tumor induced angiogenesis model. The parameter values have their usual meaning

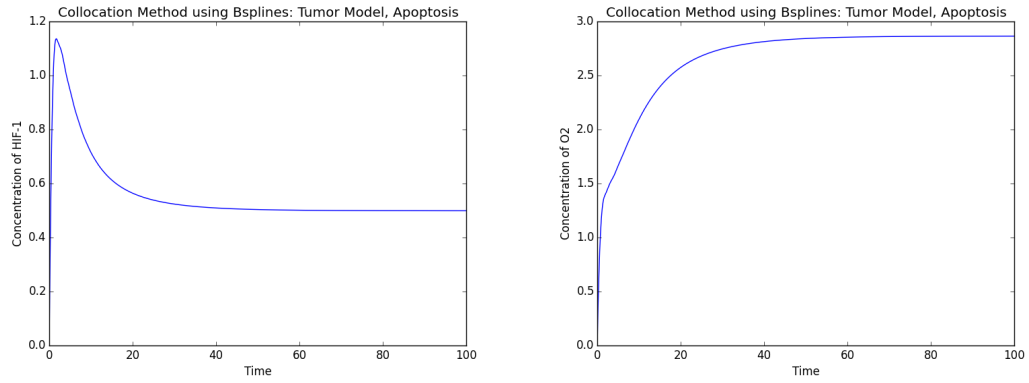

Figure 9: *Solution profile for HIF-1 and O_2.*

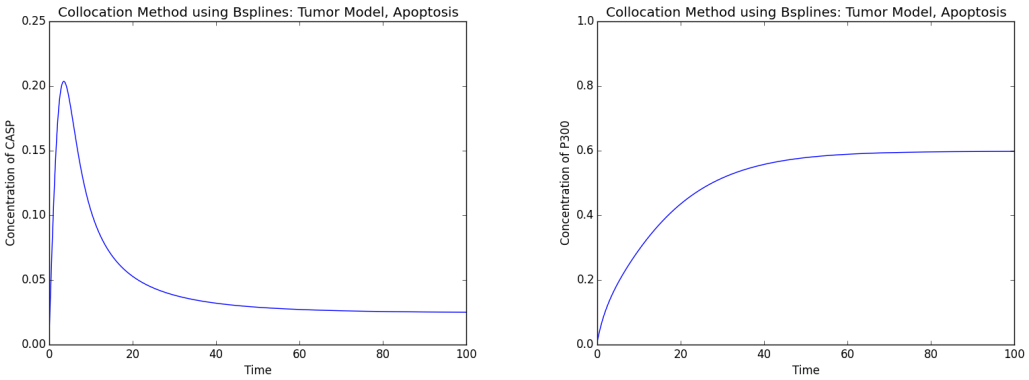

Figure 10: *Solution profile for CASP and P300.*

as explained in chapter 2. Here because of the nonlinear terms in rational form, our B-spline method could capture precisely the solution profile. We however used the python solver dopri5 to obtain the solutions. This is because compared to the other solvers for the test case problem, dopri5 had the best approximation to equation (50). The results for the reaction equations for the multiscale model were obtained

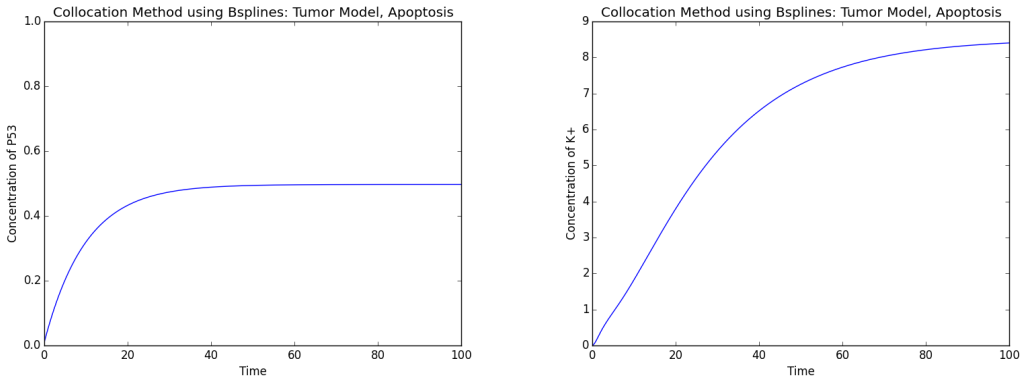

Figure 11: *Solution profile for P53 and* K^+.

as follows;

$$
\begin{aligned}
\frac{du_1(t)}{dt} &= a_1 - a_2u_2u_1 - a_3u_1u_3 - a_4u_4u_1, \\
\frac{du_2(t)}{dt} &= a_5 - a_2u_2u_1 + a_3u_1u_3 - a_6u_2, \\
\frac{du_3(t)}{dt} &= -a_3u_1u_3 - a_7u_3u_4 + a_8, \\
\frac{du_4(t)}{dt} &= -a_7u_4u_3 + a_9 - a_{10}u_4, \\
\frac{du_5(t)}{dt} &= a_{10}u_4 - a_{11}u_5u_6 + a_{12} - a_{13}u_5, \\
\frac{du_6(t)}{dt} &= -a_{11}u_5u_6 + a_6u_2 - a_{14}u_6, \\
\frac{du_7(t)}{dt} &= k_1u_7(1-u_7) - k_2u_7u_9, \\
\frac{du_8(t)}{dt} &= \frac{k_2u_8u_9}{1+u_9} - k_4u_8u_9 - k_5u_8 + k_6u_8u_{10}, \\
\frac{du_9(t)}{dt} &= k_7u_9(1-u_9) - k_8u_9u_7 - k_9u_9u_8 + \frac{k_{10}u_9u_{10}}{1+u_{10}} - \eta u_5u_9, \\
\frac{du_{10}(t)}{dt} &= \frac{k_{11}u_9u_{10}}{1+u_9} - k_{12}u_{10} + \xi u_1u_{10}.
\end{aligned}
$$

The following are the solution profiles for the 10 state variables for the multiscale model.

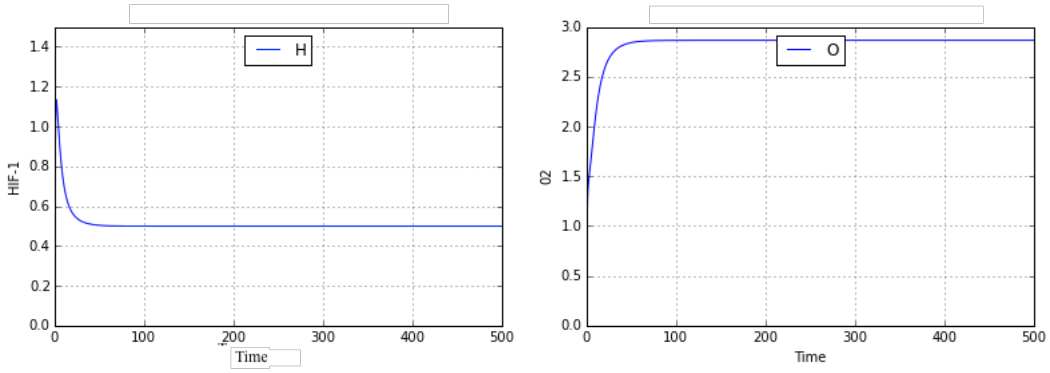

Figure 12: *Solution to multiscale tumor angiogenesis model. The graph on the left shows the solution profile of HIF whiles the graph on the right shows the solution profile of* O_2

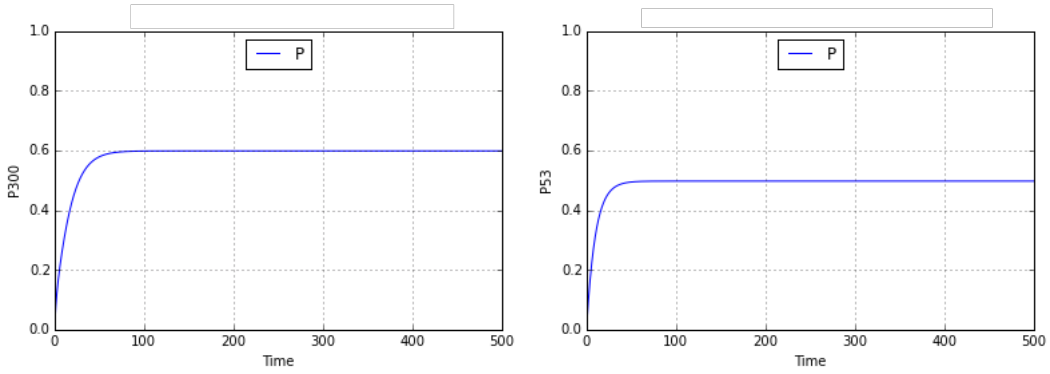

Figure 13: *Solution to multiscale tumor angiogenesis model. The graph on the left shows the solution profile of P300 whiles the graph on the right shows the solution profile of P53*

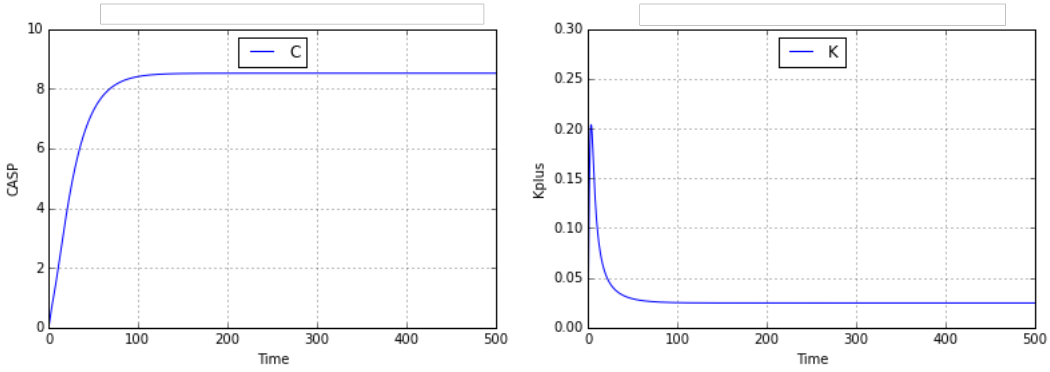

Figure 14: *Solution to multiscale tumor angiogenesis model. The graph on the left shows the solution profile of CASP whiles the graph on the right shows the solution profile of* K^+

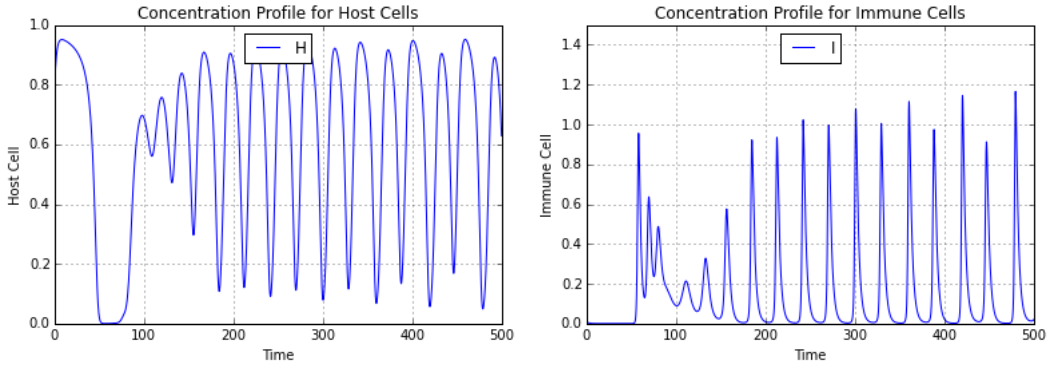

Figure 15: *Solution to multiscale tumor angiogenesis model. The graph on the left shows the solution profile of host cells whiles the graph on the right shows the solution profile of immune cells.*

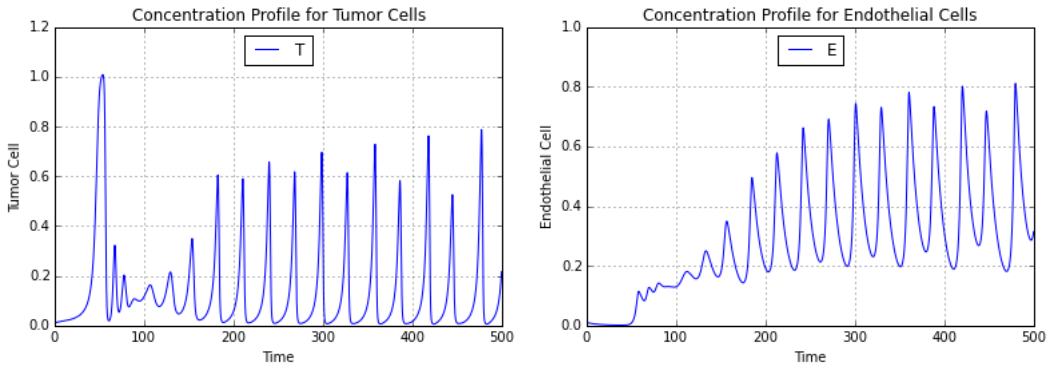

Figure 16: *Solution to multiscale tumor angiogenesis model. The graph on the left shows the solution profile of host cells whiles the graph on the right shows the solution profile of immune cells.*

5.5 Computational Algorithm for B-spline Collocation Method: Partial Differential Equations

To approximate partial differential equations using B-splines we adapt the elegance of tensor products to help us in the space and time discretization. The following is our algorithm for finding numerical approximation for partial differential equations.

Algorithm 5.3: B-spline Collocation Method for PDEs.

- 1. Create the basis matrix using collocation points in the x and t directions. The degree and knot vector is required when creating the basis matrix.
- 2. Depending on the order of the partial differential equation, the nth derivative of the basis matrix can be taken.
- 3. If the equation has a partial derivative in x then to obtain the correct partial derivative, take the tensor product between the nth order derivative matrix and the basis matrix of t.

- 4. Formulate a discretized form the PDE with the various tensor products appropriately taken in the required direction according to the structure of the PDE.

- 5. If the problem is formulated as an initial value PDE then we code the initial value function as a sub-function to be used in the solution process.

- 6. As in the case of the ODE, because the initial condition is known, we replace the sub-matrix row in V with the original sub-matrix row in for the tensor product Kron(Bt,Bx) from the first row to the length of the collocation points used in the discretization.

- 7. If the problem has boundary values, set the boundaries by replacing every first and last row in V with the rows from the tensor products for the boundary condition at a and the boundary condition at point b.

- 8. Multiply V by its transpose if V is not square and solve for c using a linear solver. Graph results and check with an analytical solution.

5.6 B-spline Collocation Method for Semi-linear Partial Differential Equations

Lastly we demonstrate how to solve semi-linear partial differential equations using the B-spline collocation method. The Algorithm we used in achieving this results is as follows;

Algorithm 5.4: B-spline Collocation Method for PDEs.

- 1. Write the left hand side operator using tensor products obtained from the basis and differential matrix
- 2. The expression for the left hand side using the B-spline approximation for the gradient function.
- 3. Setup the initial condition vector depending on the number of equations given.
- 4. Define the non linear part of the equation as a function.
- For example if there are $n-equation$, then we will have $n-nonlinear functions$
- 5. Create a PDE function to be used in solving the system of algebraic equations resulting from the B-spline discretization.
- 7. Use the initial guess to obtain the initial B-spline coefficients.
- 8. Setup a boundary fixer. The boundary fixer ensures that the boundary conditions remain the same as the solution is solved.
- 9. Using an appropriate solver in python solve the system over the desired time span. The resulting solution is the desired coefficients
- 10. Use the coefficients to write the B-spline approximation for the system and graph results.

Consider the multiscale reaction-diffusion model for the tumor angiogenesis, this model describes spatial interaction between host cells, effector immune cells, tumor

cells, endothelial cells at the cellular level. It also includes subcellular interactions, between, $HIF-1$, O_2, P300, P53, Caspases and Potassium. We assume the model is defined on a square domain with Neumann boundary conditions. The model parameters and state variables are described in detail in chapter 2.

$$
\begin{aligned}
\frac{\partial u_1(t)}{\partial t} &= d_1\nabla^2 u_1 + a_1 - a_2u_2u_1 - a_3u_1u_3 - a_4u_4u_1 \\
\frac{\partial u_2(t)}{\partial t} &= d_2\nabla^2 u_2 + a_5 - a_2u_2u_1 + a_3u_1u_3 - a_6u_2 \\
\frac{\partial u_3(t)}{\partial t} &= d_3\nabla^2 u_3 - a_3u_1u_3 - a_7u_3u_4 + a_8 \\
\frac{\partial u_4(t)}{\partial t} &= d_4\nabla^2 u_4 - a_7u_4u_3 + a_9 - a_{10}u_4 \\
\frac{\partial u_5(t)}{\partial t} &= d_5\nabla^2 u_5 + a_{10}u_4 - a_{11}u_5u_6 + a_{12} - a_{13}u_5 \\
\frac{\partial u_6(t)}{\partial t} &= d_6\nabla^2 u_6 - a_{11}u_5u_6 + a_6u_2 - a_{14}u_6 \\
\frac{\partial u_7(t)}{\partial t} &= d_7\nabla^2 u_7 + k_1u_7(1-u_7) - k_2u_7u_9 \\
\frac{\partial u_8(t)}{\partial t} &= d_8\nabla^2 u_8 + \frac{k_2u_8u_9}{1+u_9} - k_4u_8u_9 - k_5u_8 + \frac{k_6u_8u_{10}}{1+u_{10}} \\
\frac{\partial u_9(t)}{\partial t} &= d_9\nabla^2 u_9 + k_7u_9(1-u_9) - k_8u_9u_7 - k_9u_9u_8 + \frac{k_{10}u_9u_{10}}{1+u_{10}} - \eta u_5u_9 \\
\frac{\partial u_{10}(t)}{\partial t} &= d_{10}\nabla^2 u_{10} + \frac{k_{11}u_9u_{10}}{1+u_9} - k_{12}u_{10} + \frac{\xi u_1u_{10}}{1+u_1}
\end{aligned}
$$

We obtained the following results from solving the system using B-spline collocation method;

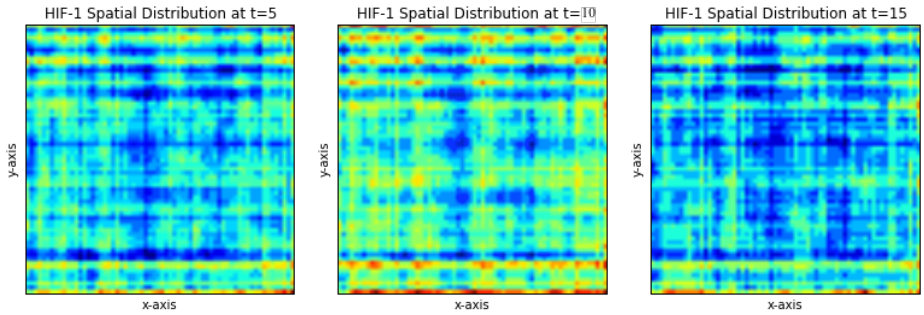

Figure 17: *Reaction diffusion solution for HIF-1 in space at different times.*

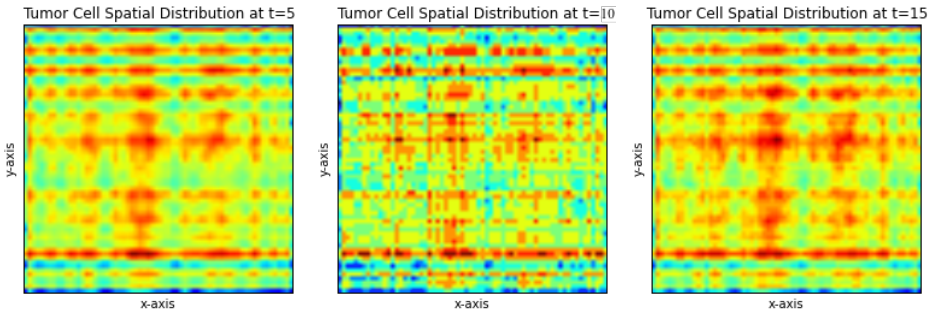

Figure 18: *Reaction diffusion solution for tumor cell concentration in space at different times.*

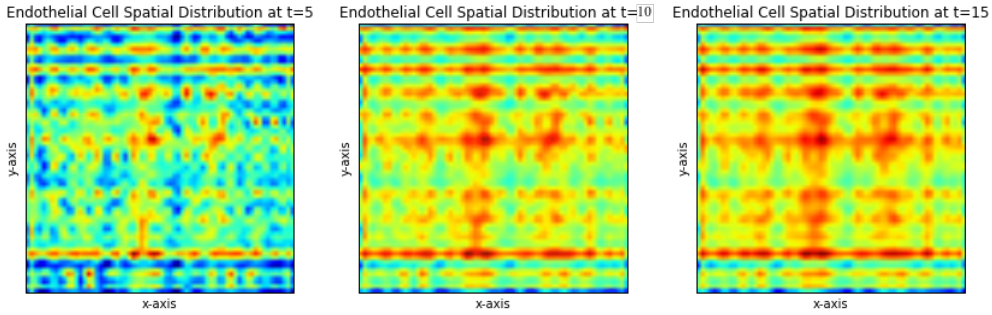

Figure 19: *Reaction diffusion solution for Endothelial cell concentration in space at different times.*

CHAPTER 6

UNCERTAINTY QUANTIFICATION AND SENSITIVITY ANALYSIS

So far we have assumed that the model parameters of reaction diffusion systems are known. But most biological parameters are uncertain or variable. We will quantify the uncertainty in the solution of the system using statistics such as mean and variance. To compute mean and variance we must compute multiple integrals. These do not have, in general, closed form solutions. Quadrature methods are used to compute integrals numerically. This method for uncertainty quantification becomes more computationally intensive as the dimensionality of the parameter space gets larger. One way of overcoming this obstacle is to apply sensitivity analysis methods to the system of random differential equations. Sensitivity analysis helps us to rank sensitivity of parameters for the system. Then we choose the top ranked parameters as uncertain and the remaining parameters as fixed in performing uncertainty and sensitivity analysis.

The most popular method for uncertainty quantification is the Monte Carlo method. The reason why the method is very popular is because it is stable [16]. The drawback is that it is computationally inefficient due to its low convergence rate. In this chapter we discuss a method for uncertainty quantification which is moderately stable and highly efficient.

We discuss uncertainty quantification without diffusion parameters. The same approach can be extended when diffusion rates are included. In the next section, we discuss the necessary definitions and preliminaries for sensitivity analysis and uncertainty quantification.

6.1 Definitions and Preliminaries

In order to perform uncertainty and sensitivity analysis, we need an efficient sampling numerical quadrature method that can be used to compute the mean and variance and determine distributions and uncertainty bounds for the model output. The higher the dimensionality of the parameters, the more computationally expensive to perform uncertainty quantification. Thus we require sensitivity analysis to reduce the number of parameters under consideration. Next we discuss preliminaries and definitions of sensitivity analysis.

One of the aims of sensitivity analysis is to quantify the relative contribution of individual parameters to variability in the model output. The reasons for sensitivity analysis include the following;

1. Determine whether the model is robust or fragile with regards to various parameters.

2. Determine whether the model can be simplified by eliminating processes that involve insensitive parameters.

The methods for sensitivity analysis are classified as local and global.

Local sensitivity is the study of how the variation in the output of a model depends on the model's input. For the purpose of parameter selection, each parameter associated with the probability distribution is sampled N times in order to generate N vectors of the parameters. The model is evaluated for each set of parameter vector and the model output is recorded. Sensitivity analysis is used to rank the input parameters according to their influence on the output. There are different types of sensitivity analysis, including qualitative and quantitative sensitivity analysis methods. Qualitative sensitivity methods include correlation analysis (CA), regression analysis (RA)

and Gaussian process(GP) [15]. Quantitative Sensitivity analysis methodsinclude elementary effects sensitivity screening analysis method, fourier amplitude sensitivity analysis (Fast), multivariate adaptive regression spline (MARS), delta test (DT) and sum of trees (SOT) [65]. We use the elementary effects sensitive screening analysis to reduce the dimension of the parameter space for the multiscale tumor angiogenesis model.

6.2 The Elementary Effects Screening Method

The elementary effect for the i-th input variable at $[0,1]^k$ is the first difference approximation to the derivative of f at x:

$$EE_i(\mathbf{x}) = \frac{f(x + he_i) - f(x)}{h}$$

where h is a small fixed positive real number, e_i is the unit vector in the direction of the i-th axis and f is the model output [15]. This is a local measure of sensitivity The average $EE_i(x)$ for various points x in the input domain may be calculated in order to obtain a more global measure of the relative influence of each factor

$$\mu_i = \frac{1}{r}\sum_{j=1}^{r} EE_i(x_j).$$

In calculating the elementary effect of the input parameter, only a single parameter is varied at a time, thus this method does not detect interactions between the input parameters.

Definition 6.16 *Local methods consider how the output changes about a base point. These methods may vary many parameters or a single parameter. Global methods on the other hand characterize how the model output depends on the model inputs over a wide range of input variables*

Some global sensitive analysis methods are based on analysis of variance (often using Monte Carlo methods). The sensitivity indices of the parameters quantify the impact that the parameter has on the output uncertainty [65]. It measures the part of the output variance which can be attributed to variability in the parameter. We note that the sensitivity index has the following properties;

1. Each index has a value $S_i \in [0,1],\ i = 1, 2, \ldots, n_p$, where n_p is the number of parameters under consideration.

2. $\sum_i^{n_p} S_i = 1$,

where the first-oder index which measures the main effect is given as

$$S_j = \frac{\mathrm{Var}(\mathbb{E}[z|x_j])}{\mathrm{var}(z)}$$

where x is the parameter and z is the output. The total effect index, that measures the residual variability due to interactions between x_i and other parameters is

$$S_{T_j} = \frac{\mathbb{E}[\mathrm{var}(z|x_j)]}{\mathrm{var}(z)}.$$

The sensitivity indices S_1 is a collection of all contains the first-order sensitivity indices, which tell us how much each input variable contribute to the overall output variability function over the domain and S_T contains the total indices, which include the interaction effects with other variables. A second order index $s_{i,j}$ tells us the level of interaction effects between x_i and x_j whiles a third order index $s_{i,j,k}$ tells us the level of interaction between the three parameters x_i, x_j and x_k. We use Sobols method for the global sensitive analysis.

6.3 Sobol's Method of Sensitivity Analysis

Sobol's method is one of the most established and widely used methods of sensitivity analysis, capable of computing the total sensitivity indicies (TSI) [65]. TSI measures the main effects of individual parameter and all the interactions (of any order) involving that parameter [65]. For example, if there are three input parameters say, A, B, and C, then the total effect of parameter A on the output is given as,

$$TS(A) = S(A) + S(AB) + S(AC) + S(ABC),$$

where $TS(i)$ is the total sensitivity index of parameter i and $S(Aj)$ denotes the second-order sensitivity index for the parameter A and j (for $j \neq A$). Sobol's method uses the decomposition of variance to calculate the Sobol's sensitivity indices [65]. The basis of the method is the decomposition of the model output function $y = f(x)$ into summands of variance using combinations of input parameters in increasing dimensionality. This can be used to determine the sensitivity of the output to the variation of an input parameter with input parameter space given as $[0,1]^k$ [65]. The main idea behind Sobol's approach for computation of sensitivity indices is the decomposition of the function $f(x)$ into summands of increasing dimensionality:

$$f(x_1,..,x_k) = f_0 + \sum_{i=1}^{k} f_i(x_i) + \sum_{1\leq i<j\leq k} f_{ij}(x_i,x_j) + ... + f_{1,2,3,..,k}(x_1,..,x_k). \quad (64)$$

The expansion of $f(x)$ is called an Anova-representation of $f(x)$ if:

$$\int_0^1 f_{i_1,i_2,i_3,..,i_s}(x_{i_1},..,x_{i_s})dx_k = 0 \text{ for } k = i_1,...,i_s. \quad (65)$$

A consequence of (65) is that all summands in (64) are orthogonal: if $(i_1,...,i_s) \neq (j_1,...,j_l)$, then

$$\int_{[0,1]^k} f_{i_1,i_2,i_3,..,i_s} f_{j_1,..,j_l} dx = 0. \quad (66)$$

Since at least one of the indices will not be repeated, the corresponding integral will vanish due to (65). It follows that if the x are random variables uniformly distributed in $[0,1]^k$, then $f(x)$ is a random variable and its expectation and variance given specific variable combinations can be computed as follows:

$$\int_{[0,1]^k} f(x)dx = f_0$$

$$\int f(x) \prod_{k \neq i} dx_k = f_0 + f_i(x_i)$$

$$\int f(x) \prod_{k \neq i,j} dx_k = f_0 + f_i(x_i) + f_j(x_j) + f_{ij}(x_i, x_j)$$

and $f_{i_1,..i_s}(x_{i_1}, ..., x_{i_s})$ are be random variables with variance D and $D_{i_1,...,i_s}$. The sensitivity indices are thus defined as the ratios

$$S(i_1, ..., i_s) = S_{i_1,...,i_s} = \frac{D_{i_1,...,i_s}}{D},$$

known as the global sensitivity indices. S_i is the first-order sensitivity index for factor x_i, which measures the main effects of x_i on the output (the partial contribution of i to the variance of $f(x)$). Similarly, S_{ij}, for $i \neq j$ is called the second-order sensitivity index. In addition, we have that

$$\sum_{s=1}^{k} S_s + \sum_{1 \leq i < j \leq k} S_{ij} + ... + S_{1,2,...,k} = 1$$

6.3.1 Application of Sobel's Method

Sobols method is relatively easy to implement using Monte Carlo based integration

$$f_0 = E(f(x)) \approx \frac{1}{N} \sum_{k=1}^{N} f(x_k),$$

$$D = \int f^2(x)dx - f_0^2 \approx \frac{1}{N} \sum_{k=1}^{N} f^2(x_k) - f_0^2,$$

$$D_i = D - \frac{1}{2}\int [f(x) - f(x_i', x_i)]^2 dx dx'_{-i},$$

$$\approx D - \frac{1}{2N}\sum_{k=1}^{N}[f(x_k) - f(x'_{ik}, x_{-ik})]^2,$$

$$D_i^{\text{tot}} = \frac{1}{2}\int [f(x) - f(x_i', x_i)]^2 dx dx'_{-i} \approx \frac{1}{2N}\sum_{k=1}^{N}[f(x_k) - f(x'_{ik}, x_{-ik})]^2,$$

Compute total sensitivity effects for the three parameters using

$$D_i^{\text{tot}} = \frac{1}{2}\int [f(x) - f(x_i', x_i)]^2 dx dx'_{-i} \approx \frac{1}{2N}\sum_{k=1}^{N}[f(x_k) - f(x'_{ik}, x_{-ik})]^2$$

sort the parameters according to their sensitivities. Here recall that the purpose of sensitive analysis is to reduce the number of parameters in order to scale down the computational complexity for performing uncertainty quantification.

6.4 Uncertainty Quantification

After the sensitive analysis we reduce the parameter space within which to perform uncertainty quantification. In general we can compute mean and variance using Monte Carlo integration. However Monte Carlo method is not efficient. As an alternative

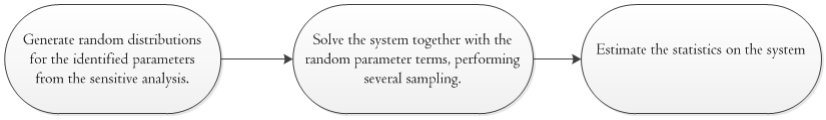

Figure 20: *This figure describes the pipeline for performing uncerntainty quantification.*

to Monte Carlo simulation, we consider orthogonal polynomials such as Lagrange or Legendre polynomial to compute the mean and variance. The solutions of the differential equations are approximated using orthogonal polynomials,

$$u \approx \hat{u}_M(t;k) = \sum_{n=0}^{N} c_n(t) P_n(k), \;\; N = M + 1$$

like Lagrange and Legendre polynomials where c_n are the polynomial coefficients, and P_k are the Lagrange or Legendre polynomials. The interpolation has much better convergence than the naive Monte Carlo method [15]. However if N is large, the approximation becomes inefficient [16]. So we need a better polynomial approximation. In the next section we discuss polynomial chaos which can be used to achieve a better polynomial approximation.

6.5 Polynomial Chaos

We seek an ideal polynomial expansion

$$u(x,a,k) \approx \hat{u}(t,a,k) = \sum_{n=0}^{K} c_n(t) P_n(a,k), K = M+1 \tag{67}$$

to resolve the associated inefficiencies associated with using Lagrange and Legendre polynomials to approximate the mean and the variance. In order to obtain a better polynomial expansion, we need to define first the structure (inner product and norm) of the solution space for such a polynomial. We define, inner product spaces weighted with probability distributions,

$$\begin{aligned} \langle u, v \rangle_Q &= E(u,v) \\ &= \int f_Q(q) u(t,q) v(t,q)\, dq \end{aligned}$$

and its associated norm

$$\|u\|_Q = \sqrt{\langle u, v \rangle}$$

where $Q = (a, k)$ is a random parameter vector. We define next when two polynomials in the expansion of the solution u are orthogonal;

$$\langle P_n, P_m \rangle_Q = \begin{cases} \|P_n\|_Q^2 & n = m, \\ 0 & m \neq n. \end{cases}$$

In the expansion (67) we define the coefficients through least squares minimization $\min_{c_0,\ldots,c_N} \|u - u_M\|^2$ such that

$$\begin{aligned} \left\langle \sum_{n=0}^{N} c_n P_n, P_k \right\rangle, &= \sum_{n=0}^{N} c_n \langle P_n, P_k \rangle_Q, \text{ k = 0,. . . ,N,} \\ &= c_k \langle P_k, P_k \rangle_Q, \end{aligned}$$

where

$$c_k = \frac{\langle u, P_k \rangle}{\|P_k\|_Q^2}$$

are known as the fourier coefficients. Minimizing the least squares is equivalent to the minimization of the variances;

$$\begin{aligned} (c_0, \ldots, c_N) &= \underset{c_0,\ldots,c_N}{\text{argmin}} \|u - \hat{u}_M\|_Q, \\ &= \underset{c_0,\ldots,c_N}{\text{argmin}} \|u - \hat{u}_M\|_Q^2, \\ &= \underset{c_0,\ldots,c_N}{\text{argmin}} E((u - \hat{u}_M)^2), \\ &= \underset{c_0,\ldots,c_N}{\text{argmin}} Var(u - \hat{u}_M). \end{aligned}$$

If the polynomials in the expansion of the approximate solutions are orthogonal then we can calculate mean and variance as follows;

$$\begin{aligned} E(\hat{u}_M) &= E\left(\sum_{n=0}^{N} c_n P_n\right), \\ &= \sum_{n=0}^{N} c_n E(P_n), \\ &= \sum_{n=0}^{N} c_n \langle P_n, P_0 \rangle_Q, \\ &= c_0, \end{aligned}$$

and

$$\begin{aligned} Var(\hat{u}_M) &= Var\left(\sum_{n=0}^{N} c_n P_n\right) \\ &= \sum_{\substack{n=0 \\ m=0}}^{N} c_n c_m (E(P_n P_m) - E(P_n)E(P_m), \\ &= \sum_{\substack{n=0 \\ m=0}}^{N} c_n c_m \langle P_n, P_m \rangle_Q - c_0^2, \\ &= \sum_{n=1}^{N} c_n^2 \|P_n\|_Q. \end{aligned}$$

Now we can construct an orthogonal polynomial expansion using Gram-Schmidt orthogonalization as follows;

$$\begin{aligned} P_0 &= v_0, \\ P_n &= v_n - \sum_{m=0}^{n-1} \frac{\langle v_n, P_m \rangle_Q}{\|P_m\|_Q^2}, \\ &= v_n - \sum_{m=0}^{n-1} \frac{E(v_n, P_m)}{E(P_m^2)}. \end{aligned}$$

Gram-Schmidt method is known to be unstable for higher order polynomial terms [16]. This is because the vandermonde matrix associated with the polynomials are

ill-conditioned. Thus Gram-Schmidt orthogonalization is not enough.

We find that a better way of numerically constructing the orthogonal polynomials is through the three-term discretized Stiltjes recursion. This method is stable and has a recursion relation is given as:

$$P_{n+1} = (x - A_n)P_n - B_n P_{n-1},\ P_{-1} = 0\ \ P_0 = 1,$$

where

$$A_n = \frac{\langle qP_n, P_n \rangle_Q}{\|P_n\|_Q^2}$$

and

$$B_n = \begin{cases} \dfrac{\|P_n\|_Q^2}{\|P_{n-1}\|_Q^2} & n > 0, \\ \\ \|P_n\|_Q^2 & n = 0, \end{cases}$$

$$\begin{aligned} \langle P_n, P_m \rangle_Q &= E\left(P_n^{(1)} \dots P_{nD}^{(D)} \cdot P_m^{(1)} \dots P_{mD}^{(D)}\right), \\ &= E\left(P_{n1}^{(1)} \cdot P_{m1}^{(1)}\right) \dots E\left(P_{nD}^{(D)} \cdot P_{mD}^{(D)}\right), \\ &= \left\langle P_{n1}^1, P_{m1}^1 \right\rangle_Q \dots \left\langle P_{nD}^D, P_{mD}^D \right\rangle_Q. \end{aligned}$$

6.6 Application of Sensitive Analysis and Uncertainty Quantification to Multiscale Model

We begin by obtaining the right parameter set by using data from [32] described in table (4). We performed the parameter estimation using the method discussed [60]. Having obtained the appropriate parameter sets, we performed local sensitivity analysis using the elementary effects screening method. The output in figure (6.6) shows the ranking for the most sensitive parameters.

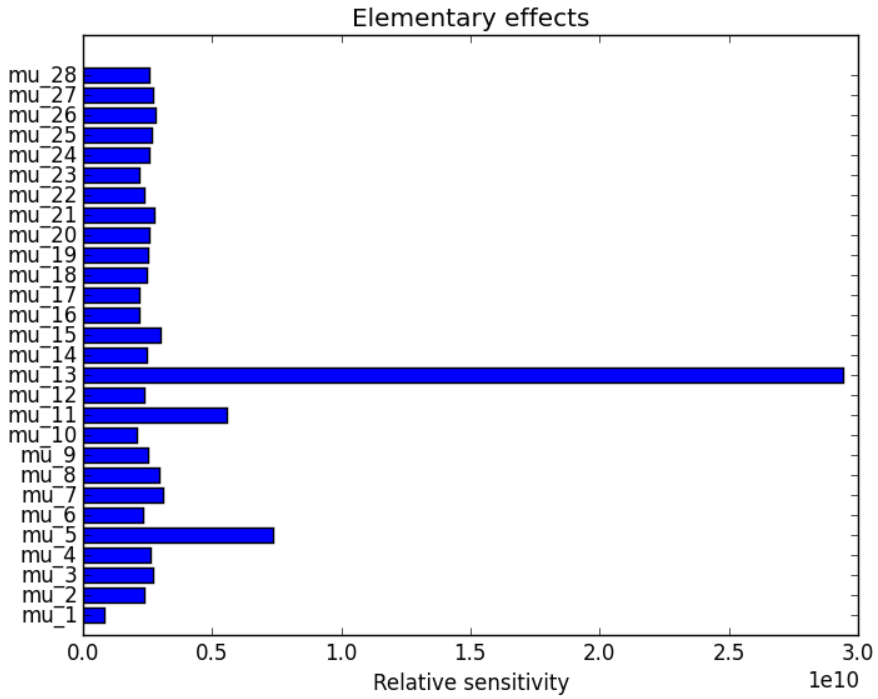

Figure 21: *Relative sensitivitiy rank for the multiscale tumor angiogenesis model. The results shows that the parameters,* a_5, a_{11}, a_{13} *and* ρ_1 *from the multiscale model are the most sensitive.*

We used next the Sobol's method with uniform parameter range to further screen the parameters to reveal the parameter that have the most influence on the model outcome. Applying the Sobol's method we got the results in Table (5).

Lastly we performed uncertainty quantification on the multiscale model where the high ranked parameters a_5 and a_{11} are varied. We obtained the following solution profiles for each of the state variables in the multiscale model;

Table 4: *Time course data for Caspases gene expression [32].*

Time	$15min$	$30min$	$1h$	$2h$	3 h	4 h	5h	6h	7 h	8h
$CASP4$	0.97	0.69	1.87	0.79	1.23	2.22	1.32	1.07	1.57	1.19
$CASP6$	1.15	0.76	1.23	0.87	1.00	1.42	1.23	0.93	1.37	1.32
$CASP7$	1.07	0.79	1.11	0.79	1.52	1.01	1.04	0.93	1.15	0.87
$CASP9$	1.04	0.87	1.28	0.62	1.32	1.68	1.07	1.11	1.63	1.57

Time	8 h	9h	10 h	12 h	24 h	36 h	48 h	60 h	72 h
CASP 4	1.19	1.23	0.84	4.61	2.3	0.73	1.07	0.45	1.07
CASP 6	1.32	1.46	1.19	2.22	1.19	0.68	1.19	0.56	1.15
CASP 7	0.87	1.00	1.07	2.46	2.55	0.93	1.46	0.45	0.97
CASP 9	1.57	1.68	1.47	1.75	1.15	1.32	1.75	1.00	1.37

Table 5: *First order and total sensitivity index for multiscale model using Sobol's method. The parameters a_5, a_{11}, a_{13} and ρ_1 from the elementary sensitivity test were the only parameters considered in the Sobol's analysis.*

Parameter	S_1	S_1 Conf	S_T	S_T Conf
a_5	0.00	0.00198	0.000731	0.000289
a_{11}	1.00	0.25438	0.997793	0.051659
a_{13}	0.00	0.00014	0.000008	0.000006
ρ_1	0.00	0.00000	0.000000	0.000000

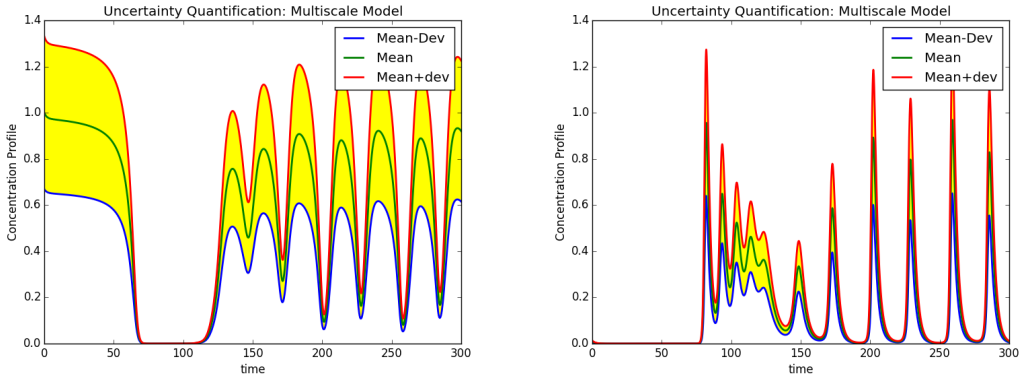

Figure 22: *The figure on the left represents the solution profile for host cells exhibiting Jeff's phenomenon, whiles the figure on the right represents the solution profile for immune cells exhibiting Jeff's phenomenon in the multiscale model.*

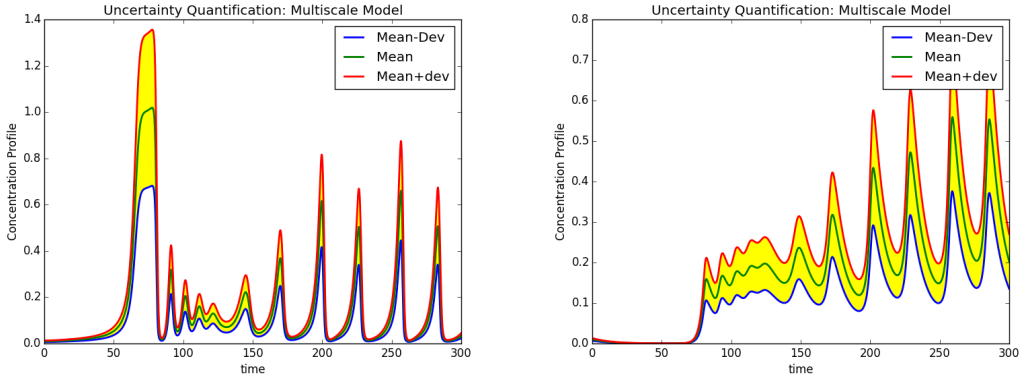

Figure 23: *The figure on the left represents the solution profile for tumor cells exhibiting Jeff's phenomenon, whiles the figure on the right represents the solution profile for endothelial cells exhibiting Jeff's phenomenon in the multiscale model.*

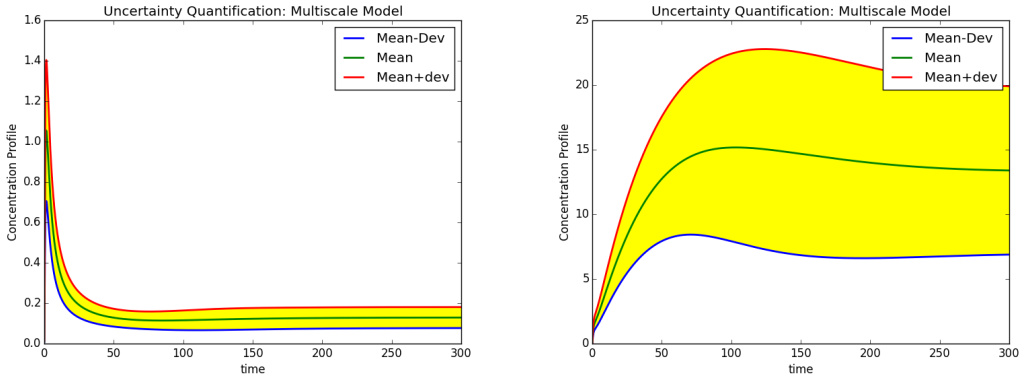

Figure 24: *The figure on the left represents the solution profile for HIF-1, whiles the figure on the right represents the solution profile for O_2 concentration in the multiscale model.*

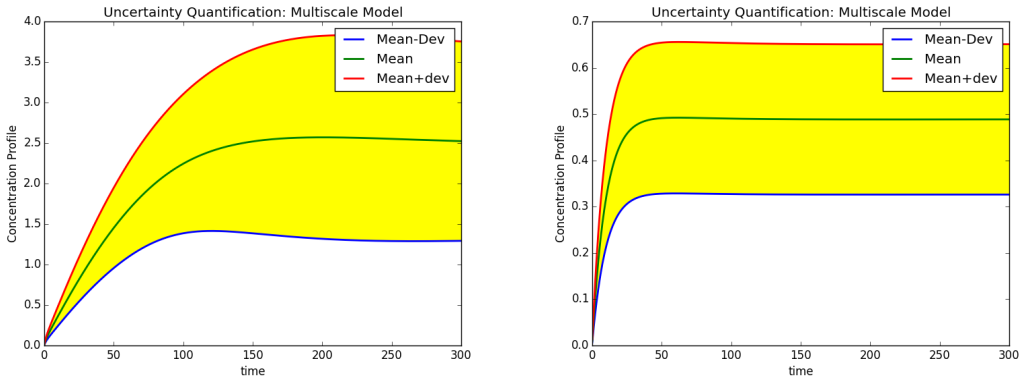

Figure 25: *The figure on the left represents the solution profile for P300 coactivator, whiles the figure on the right represents the solution profile for P53 gene concentration in the multiscale model.*

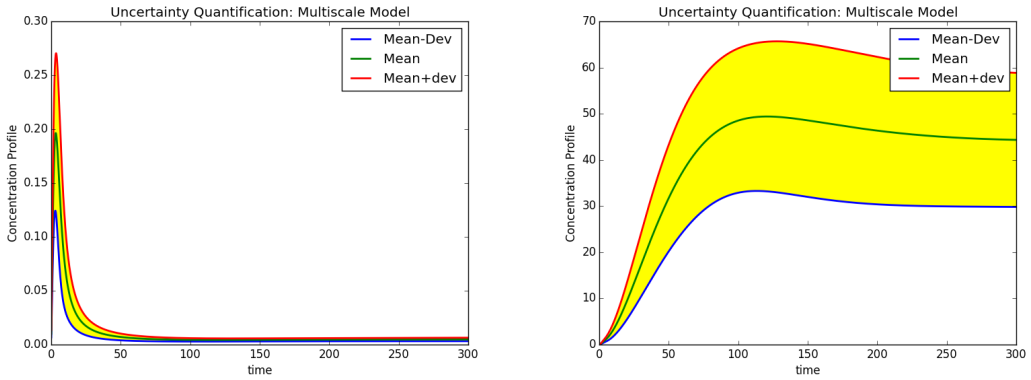

Figure 26: *The figure on the left represents the solution profile for Caspases, whiles the figure on the right represents the solution profile for Potassium gene concentration in the multiscale model.*

6.7 A Discrete Stochastic Model for Blood Vessel Growth

The draw back of the continuum models is lack of actually representing the blood vessels distribution in response to angiogenesis. In order to do this, we couple a discrete stochastic equation in predicting the vascular network to the multiscale model

presented above. In this model [46, 59], we use a random diffusion term to control the random movement of the endothelial cell tips instead of the rotation matrix used in [14, 31]. In the discrete model the ith subscript denotes the state of the ith blood vessel sprout. The model is comprised of a deterministic tip equation given as;

$$\frac{dx_i}{dt} = v_i(t),$$

whiles the movement of the tip velocity is governed by a stochastic differential equation given as;

$$dv_i(t) = -\beta v_i(t)dt + \sqrt{\alpha}dW_i(t) + \kappa\nabla a \sin\left(\frac{\Phi}{2}\right)dt,$$

where β is the viscosity coefficient, W is the Wiener process, a white noise, a is TAF concentration, in this model we relate the TAF concentration with the multiscale reaction diffusion equation by taking a set of random numbers between the maximum and minimum TAF concentrations, Φ is the angle between the direction the tip is moving and that toward the TAF source, and i denotes ith sprout. Φ is defined more explicitly as

$$\Phi = cos^{-1}\left[\frac{(x_a - x_i)cos\theta_i + (y_a - y_i)sin\theta_i}{((x_a - x_i)^2 + (y_a - y_i)^2)^{1/2}}\right]$$

and finally the equation for the average density is

$$\frac{d\rho_i}{dt} = k_g\frac{\rho_{\max} - \rho_i(t)}{\rho_{\max} - \rho_{\min}}\rho_i(t) - \frac{s_i(t)}{L_i(t)}\rho_i(t) + k_b\left[\rho_{pv}(t) - \rho_i(t)\right] - \sum_{j=1}^{\nu_i} k_b\left[\rho_i(t) - \rho_j(t)\right]$$

where, k_g is the proliferation rate, k_b is the distribution coefficient, $\rho_{pv}(t)$ is the number of branches that the ith sprout has at time t, s_i in the instantaneous speed of the ith sprout has calculated as $s_i(t) = \|v_i(t)\|$ and L_i is the sprout length calculated from

$$\frac{dL_i}{dt} = s_i(t). \tag{68}$$

In addition, we considered the term ∇a to be a function depending on the tumor concentration from the reaction diffusion equation. We obtained the following results for the vascular network structure using the discrete stochastic differential equation

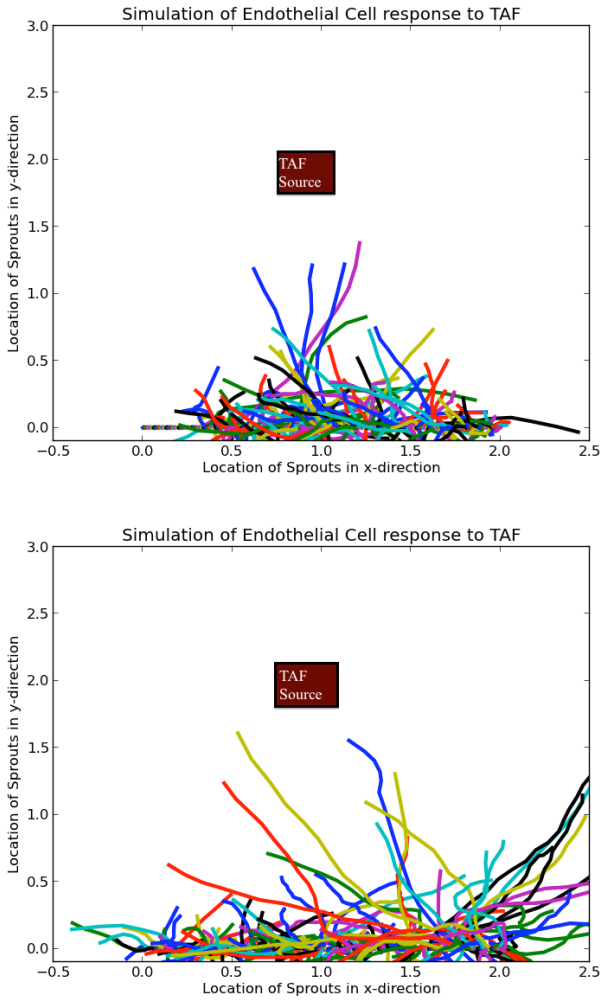

Figure 27: *Two Simulations of tumor induced angiogenesis vascular growth in response to TAF. The figure shows blood vessel sprouts at different locations responding and growing towards tumor source.*

CHAPTER 7

CONCLUSION AND FUTURE WORK

We constructed a semi-linear parabolic multiscale model for tumor angiogenesis by establishing a relation between intracellular and intercellular dynamics. We analyzed the resulting system for the existence of solution through semigroups. We showed that the system satisfies the positivity condition and mass control structure, thus ensuring that the solutions does not blow up in finite time. Having established that existence of solutions for the model, we went ahead to solve the resulting system using a B-spline collocation method.

Since most parameters in biological systems are not known or else variable, we investigated the sensitivity and uncertainty of the model output to the parameters. Since large parameter sets increase the computational complexity of performing uncertainty quantification, we reduced the parameter space (the number of parameters to consider as uncertain) by applying local and global sensitivity analysis on the reaction terms in the model. We plan to extend this concept to include the diffusion terms. Having identified the most sensitive parameters, we performed uncertainty quantification on the model with deterministic parameters and uncertain parameters, where the uncertain parameters were those identified through the sensitivity analysis.

Finally since continuum models do not capture the vascular structures in the process of angiogenesis, we solved a discrete stochastic differential equation whose chemotactic term depends on the highest and lowest tumor concentration from the multiscale model. Future work will focus on this model and provide a better coupling between the multiscale model and the growth of the blood vessels.

BIBLIOGRAPHY

[1] E. Allen, *Modeling with Ito stochastic differential equations*, Springer, Dordrecht, The Netherlands (2007).

[2] M.S. Alves, *Atrator global para o sistema de timoshenko*, Atas do 44o. Seminário Brasileiro de Análise, 597-602, (1996).

[3] Amgen, *Pioneering new frontiers in tumor angiogenesis*, Amgen Biotechnology, (2010).

[4] H. Amann, *Global existence for semilinear parabolic systems*, J. Reine Angew. Math., 360, 47-83, (1985).

[5] H. Amann, *Dynamic theory of quasilinear parabolic systems, global existence*, Math. Z. 202, 2, 219-250, 1989 and Math. Z. 205, 2, 231, (1990).

[6] H. Amann, *Highly degenerate quasilinear parabolic systems*, Ann. Scuola Sup. Pisa, Cl. Sci. (4) 18, 135-166, (1991).

[7] H. Amann, *Hopf bifurcation in quasilinear reaction diffusion systems, and delay differential equations and dynamical systems*, Lecture Notes in Math. 1475, Springer-Verlag, (1991).

[8] O. Botella, *A velocity pressure Navier-Stokes solver using Bspline collocation method*, Annu. Res. Center for Turbulence Research, 403 (1999).

[9] V. Capasso and A. Di Liddo, *Global attractivity for reaction diffusion systems. The case of non-diagonal matrices*, J. Math. Anal. Appl. 177, 510-529, (1993).

[10] M.A.J Chaplain et al, *Mathematical modeling of tumor Induced Angiogenesis*, Annu. Rev. Biomed Eng, (233-57) (2006).

[11] Conway et al, *Large time behavior of solutions of systems of nonlinear reaction diffusion equations*, SIAM Journal on Applied Mathematics vol. 35, 1 - 16, (1978).

[12] T.Deisboeck, S. Wang, Z. Macklin, P. Cristini, *Multiscale cancer modeling*, Annu. Rev. Biomed Eng., 127-55, (2011).

[13] C. De Boor, *A practical guide to splines*, Springer Verla, (1978).

[14] R. C. Ewool & Z. Sinkala, *Analysis of the mathematical model for tumor induced angiogenesis*, J. Appl. Math and Phys. 2, pp. 698 - 707, (2014).

[15] Fienberg et al, *Chaospy: an open source tool for designing methods of uncertainty quantification*, Journal of Computational Science 11, 46 -57, (2015).

[16] J. Fienberg and S. Tennoe , *Polynomial chaos expansion*, Lecture Notes, Kalkulo, AS, (2015).

[17] Frasso G, *Splines, differntial equations and optimal smoothing*, Dissertation, Universita Degli Studi Di Napli Frederico II, (2013).

[18] G. Fichera, *Analisi esistenziali per le soluzioni dei problemi al contorno misti, relativi all'equazioni e ai sistemi di equazioni del secondo ordine di tipo ellittico, autoaggiunti*, Ann. Scuola Norm. Sup. Pisa (3) 1, 75-100, (1947).

[19] G. Fichera, *Linear elliptic differential systems and eigenvalue problems*, Lecture Notes in Math. 8, Springer-Verlag, (1965).

[20] J. Folkman, *Fundamental concept of the angiogenic process*, N. Engl. J. Med, 285, pp. 1182–1186, (1971).

[21] J. Folkman, *What is the evidence that tumors are angiogenesis dependent?*, J. Natl. Cancer Inst.82 (1989).

[22] J. Folkman, *Angiogenesis in cancer, vascular rheumatoid and other diseases*, Natl. Med. 1, 27-31, (1995).

[23] J. Folkman, *Role of angiogenesis in tumor growth and metastasis*, Semin. Oncol. 29, 15 -18 (2002).

[24] E. Gerard I, K. Vousden, *Cell cycle and apoptosis in cancer*, Nature 411:342-8 (2001).

[25] D. Good, P. Polverini, F. Rastinejad, M. Le Beau, R. Lemons, W. Frazier, N. Bouck *A tumor suppressor-dependent inhibitor of angiogenesis is immunologically and functionally indistinguishable from a fragment of thrombospondin*, Proceedings of the National Academy of Sciences, 87, pp. 6624, (1990).

[26] D. Henry, *Geometric theory of semilinear parabolic equations*, Springer-Verlag, (1981).

[27] J.K. Hale, *Asymptotic behavior of dissipative systems*, AMS Mathematical Surveys and Monographs 25, Providence, RI, (1988).

[28] J.K. Hale, *Ordinary differential equations*, John Wiley & Sons Inc. New york (1969), Reprinted Dover Publicaitons, (2009).

[29] J.K. Hale, *Functional differential equations* Springer, (1979).

[30] F. Hillen and A. W. Griffioen, *Tumor vasculartization: sprouting angiogenesis and beyond*, Cancer Metastas Rev. 26, 71-73, (2007).

[31] H. A. Harrington, M. Maier, L.Naidoo, N. Whitaker, *A hybrid model for tumor-induced angiogenesis in the cornea in the presence of inhibitors*, Mathematical and Computer Modeling, Vol. 46, pp. 513-524, (2006).

[32] T. Huang et al *An apoptosis-related gene network induced by novel compound cRGD in human breast cancer cells*, FEBS Letters, 581, 3517-3522, (2007).

[33] M. Kanehisa, S. Goto, *Kyoto encyclopedia of genes and genomes*, Nucleic Acids Res. 28:27-30, (2000).

[34] J.F.R Kerr, A.H Wylie, *A basic biological phenomenon with wide-ranging implications in tissue kinetics*, Br. J. Cancer 6(4): 239-57, (1927).

[35] J.U. Kim, *On the energy decay of a linear thermoelastic bar and plate*, SIAM J. Math. Anal., vol. 23, no. 4, 889-899, (1992).

[36] H. K . Klaus, *Finite element methods with Bsplines*, SIAM, (2003).

[37] K . Kristiansen, *Reaction diffusion models in mathematical biology*, Technical universtiy of Denmark, (2008).

[38] K . Yosida, *Functional analysis*, New York, (1966).

[39] Louise Viger, Fabrice Denis, Martin Rosalie, Christophe Letellier, *A cancer model for the angiogenic switch*, Journal of Theoretical Biology 360, 21 - 33, (2014).

[40] P. Laise, D. Fanelli, A. Arcangely, *A dynamical model of apoptosis and its role in tumor progression*, Commun. Nonlinear Sci, 17, 1795 - 1804, (2012).

[41] C. Letellier, L. A. Auguirre, J. Maquet, *What can we learn from a chaotic cancer model?*, J. Theor. Biol., 322, 7 - 16, (2013).

[42] H. Leiva, *Stability of a periodic solution for a system of parabolic equations*, Applicable Analysis, vol. 60, 277-300, (1996).

[43] Z.-Y. Liu and M. Renardy, *A note on the equations of a thermoelastic plate*, Appl. Math. Letters, Vol. 8, 1-6, (1995).

[44] H. Levine, A. Tucker, M. Nilsen-Hamilton *A mathematical model for the role of cell signal transduction in the initiation and inhibition of angiogenesis* Growth Factors, 20, p. 155 (2002).

[45] R.J. LeVeque, *Finite difference methods for ordinary and partial differential equations*, SIAM, (2007).

[46] Mantzaris Nikos, Steve Webb, Hans G Otherman *Mathematical modeling of tumor-induced angiogenesis*, Journal of Mathematical Biology, Vol 49 No 2 08, p. 111-187, (2004).

[47] C. Miao and Bo Zhang *The Cauchy problem for semilinear parabolic equatons in BESOV spaces*, Houston Journal of Mathematics, Vol 30 No 3, (2004).

[48] P. M Prenter *Splines and variational methods*, John Wiley and Sons Inc. New York (1975).

[49] M. Pierre and Didier Schmitt, *Blowup in reaction diffusion systems with dissipation of mass*, SIAM Review Vol. 42 No 1. pp(93 -106), (2006).

[50] M. Pierre , *Global existence in reaction diffusion systems with control of mass: a survey*, Milan J. Math 78, 417 - 455, (2010).

[51] L.A.F. de Oliveira, *Exponential decay in thermoelasticity*, Comm. in Appl. Analysis, vol.1, 113-118, (1997).

[52] L.A.F. de Oliveira, *Instability of homogeneous periodic solutions of parabolic delay equations*, J. Diff. Eq., Vol. 110, 42-76, (1994).

[53] J. D. Murray, *Parameter space for turning instability in reaction diffusion mechanisms: a comparism of models*, J. Theor. Biol., (98) 143, (1982).

[54] P. K Maini et al, *Turing model for biological pattern formation and the robustness problem*, Interface Focus, (2) 487 - 496, (2012).

[55] F Rothe, *Global solutions of reaction diffusion systems*, Lecture Notes in Mathematics, 1072, Springer, Berlin (1984).

[56] Salsman V.S et al, *Crosstalk between medulloblastoma cells and endothelium triggers a strong chemotactic signal recruiting T. lymphocytes to the tumor microenvironment*, PLoS ONE 6. (5), (2012).

[57] Schnell et al, *Multiscale modeling in biology*, American Scientist Vol 95, (2007).

[58] D. Sevicovic, *Existence and limiting behavior for damped nonlinear evolution equations with non local terms*, Comment. Math. Univ. Carolinae, 31, 2, 283-293, (1990).

[59] C .L . Stokes, D. A .Lauffenburger, *Analysis of the roles of microvessel endothelial cell random motility and chemotaxis in angiogenesis*, J. Theor. Biol., 152, 377 - 403, (1991).

[60] Z. Sinkala, R. C Ewool *Parameter estimation of ordinary differential equations using P-spline and convex optimization*, Journal of Computational and Nonlinear Dynamics, ASME (submitted), (2016).

[61] E. D. Sontag, *Mathematical contorl theory: deterministic finite dimensional systems*, Springer, New York, pp. 481, (1998).

[62] S. Tong, F. Yuan, *Numerical simualtion of angiogeneis in the cornea*, Microvascular Research,61, pp. 14-27, (2001).

[63] M.R Young, *Endothelial cells in the eyes of an immunologist.*, Cancer Immunol. Immunother. 61 (10), 1609-1616, (2012).

[64] I. Yang, C Tomlin, *Reaction diffusion systems in protein networks: global existence and identification*, Systems and Control. 74, 50-57, (2014).

[65] X. Y. Zhang et al, *Sobol sensitivity analysis: a tool to guide the development of systems pharmacology models*, Pharmacol. 4, 69-79, (2015).